nature cell biology

Damage-induced lncRNAs control the DNA damage response through interaction with DDRNAs at individual double-strand breaks

Flavia Michelini[1], Sethuramasundaram Pitchiaya[2,5], Valerio Vitelli[1], Sheetal Sharma[1], Ubaldo Gioia[1], Fabio Pessina[1], Matteo Cabrini[3], Yejun Wang[4], Ilaria Capozzo[3], Fabio Iannelli[1], Valentina Matti[1], Sofia Francia[1,3], G. V. Shivashankar[1,4], Nils G. Walter[2] and Fabrizio d'Adda di Fagagna[1,3,6]

The DNA damage response (DDR) preserves genomic integrity. Small non-coding RNAs termed DDRNAs are generated at DNA double-strand breaks (DSBs) and are critical for DDR activation. Here we show that active DDRNAs specifically localize to their damaged homologous genomic sites in a transcription-dependent manner. Following DNA damage, RNA polymerase II (RNAPII) binds to the MRE11–RAD50–NBS1 complex, is recruited to DSBs and synthesizes damage-induced long non-coding RNAs (dilncRNAs) from and towards DNA ends. DilncRNAs act both as DDRNA precursors and by recruiting DDRNAs through RNA–RNA pairing. Together, dilncRNAs and DDRNAs fuel DDR focus formation and associate with 53BP1. Accordingly, inhibition of RNAPII prevents DDRNA recruitment, DDR activation and DNA repair. Antisense oligonucleotides matching dilncRNAs and DDRNAs impair site-specific DDR focus formation and DNA repair. We propose that DDR signalling sites, in addition to sharing a common pool of proteins, individually host a unique set of site-specific RNAs necessary for DDR activation.

Maintenance of genome integrity is vital for cells and organisms. Cells have evolved a prompt set of actions, the DNA damage response (DDR), to react to any discontinuity in their nuclear DNA. DNA double-strand breaks (DSBs) are among the most powerful activators of the DDR. DSBs are sensed by the MRE11–RAD50–NBS1 (MRN) complex, which is recruited to the lesion and activates the kinase ataxia telangiectasia mutated (ATM), leading to its auto-phosphorylation (pATM) and to the phosphorylation of histone H2AX at Ser139 (named γH2AX), a key step in DDR activation. γH2AX acts as a beacon for the secondary recruitment of additional pATM molecules and DDR proteins, such as p53-binding protein 1 (53BP1), fuelling further spreading of γH2AX and accumulation of DDR factors at DSBs in a positive feedback mechanism that results in the generation of cytologically detectable nuclear foci[1].

DDR factors and RNA transcripts can functionally interact[2]. A role for RNA has emerged in DNA repair[3–12] and genomic rearrangements[13], although not univocally[14,15]. We previously reported that the secondary recruitment of DDR factors to sites of DNA damage relies on DICER- and DROSHA-dependent generation of DSB-induced small non-coding RNAs (ncRNAs) termed DNA damage response RNAs (DDRNAs), carrying the sequence of the DNA flanking the DSB[16,17], including at dysfunctional telomeres[18]. Similar small ncRNAs were reported in *Neurospora crassa*, *Arabidopsis thaliana*, *Drosophila melanogaster* and in human cell lines[6,7,9,10,19].

At present, it is unclear whether DDRNAs are processed from pre-existing transcripts or from RNA molecules induced by DNA damage. Similarly, the mechanism by which DDRNAs control focus formation and DDR activation in a sequence-dependent manner is unclear. Here we show that DDRNA precursors, termed damage-induced long non-coding RNAs (dilncRNAs), are generated by RNA polymerase II (RNAPII) from DNA ends of DSBs. Pairing between DDRNAs and dilncRNAs allows site-specific localization of DDRNAs at the damaged site and the formation of a DDR focus, which can be site-specifically targeted with antisense oligonucleotides.

RESULTS

RNAPII-dependent site-specific localization of DDRNA

To characterize DDRNA functions, we studied their intracellular localization in NIH2/4, a mouse cell line carrying an integrated construct containing a recognition site for the I-SceI endonuclease

[1]IFOM—The FIRC Institute of Molecular Oncology, Milan 20139, Italy. [2]Single Molecule Analysis Group and Center for RNA Biomedicine, Department of Chemistry, University of Michigan, Ann Arbor, Michigan 48109-1055, USA. [3]Istituto di Genetica Molecolare, CNR - Consiglio Nazionale delle Ricerche, Pavia 27100, Italy. [4]Mechanobiology Institute, National University Singapore, 117411 Singapore, Singapore. [5]Present address: Michigan Center for Translational Pathology, University of Michigan Cancer Center, Ann Arbor, Michigan 48109-0940, USA.
[6]Correspondence should be addressed to F.d'A.d.F. (e-mail: fabrizio.dadda@ifom.eu)

Received 17 June 2017; accepted 13 October 2017; published online 27 November 2017; DOI: 10.1038/ncb3643

© 2017 Macmillan Publishers Limited, part of Springer Nature. All rights reserved.

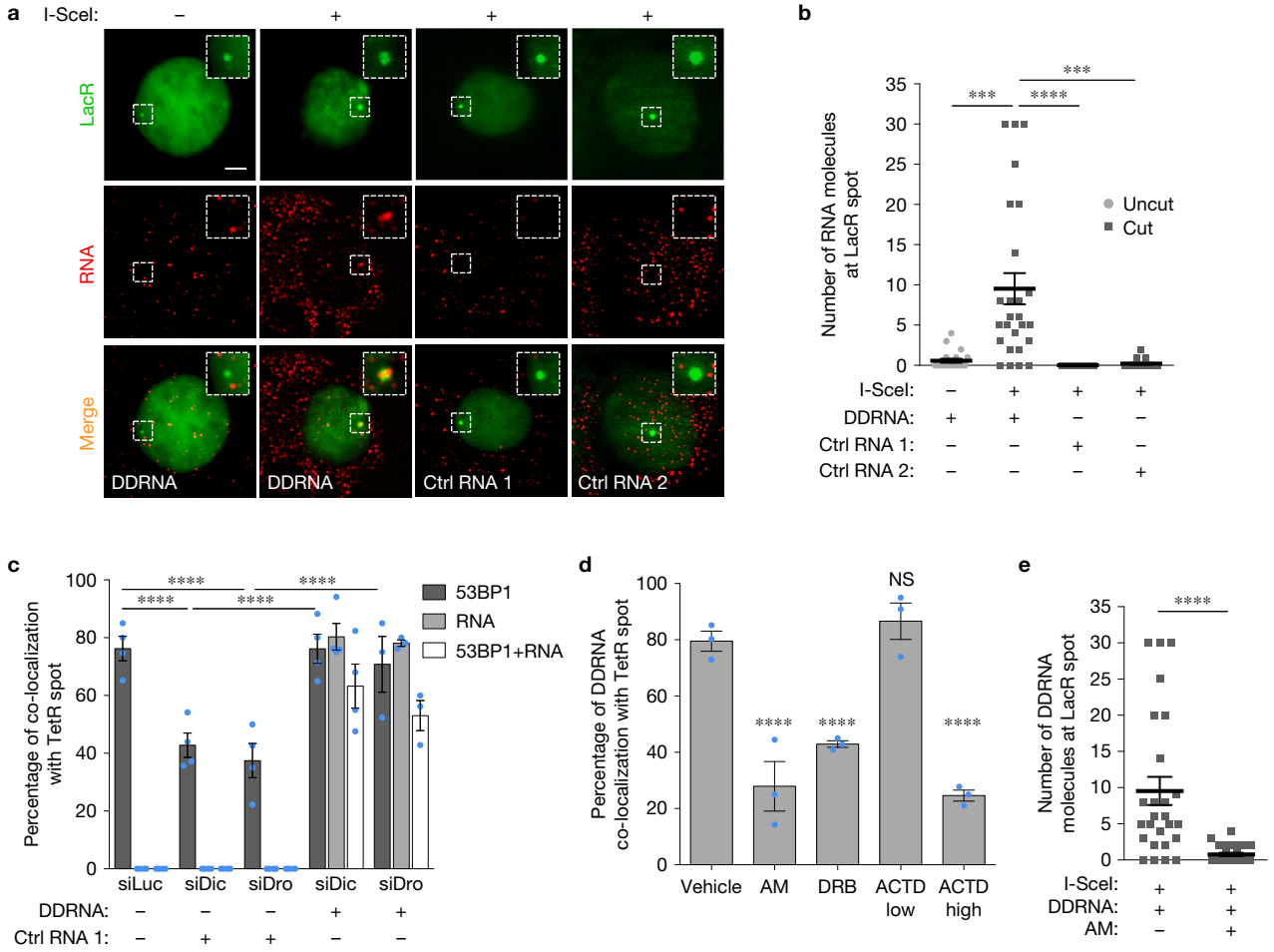

Figure 1 Sequence-specific localization of DDRNAs at DNA damage sites is transcription-dependent. (**a**) Images of NIH2/4 cells expressing GFP-LacR, microinjected with double-stranded DDRNA-Cy5, artificial CXCR4-Cy5 miRNA (Ctrl RNA 1) or let-7a-Cy5 miRNA (Ctrl RNA 2), together with BSA (−) or I-SceI restriction enzyme (+) and imaged 4 h post injection. Scale bar, 5 μm. The insets show a magnified view of the outlined region. Images from one out of three experiments with similar results. (**b**) Quantification of **a** showing the number of fluorophore-labelled RNA molecules at the locus as measured by single-molecule analysis based on stepwise photobleaching. The dots represent individual cells. The black line represents the mean ± s.e.m. (pooled data from $n=3$ independent experiments are shown). (**c**) DDRNAs localize at the damage site to restore DDR focus formation. NIH2/4 cells knocked down for Dicer and Drosha were mildly permeabilized and incubated with DDRNA-Cy5 or CXCR4-Cy5 (Ctrl RNA 1). The bar plot shows the percentage of cells positive for co-localization of 53BP1 with TetR, of RNA-Cy5 with TetR, and the triple co-localization of 53BP1, RNA-Cy5 and TetR. The error bars indicate s.e.m. (for siLuc and siDic $n=4$, for siDro $n=3$ independent experiments, ≥70 cells analysed in total per condition). (**d**) NIH2/4 cells expressing YFP-TetR and inducible I-SceI were treated with AM, DRB, ACTD at low and high doses, or vehicle alone for 2 h before cut induction, then mildly permeabilized and incubated with DDRNA-Cy5. The bar plots show the percentage of cells in which DDRNA signal co-localizes with the TetR spot. The error bars indicate s.e.m. ($n=3$ independent experiments, ≥80 cells analysed in total per condition). (**e**) NIH2/4 cells expressing GFP-LacR were microinjected with double-stranded DDRNA-Cy5, together with I-SceI protein and AM, and imaged 4 h post injection. The plot shows the number of DDRNA molecules at the locus as measured by single-molecule counting based on stepwise photobleaching. The dots represent individual cells. The black line represents the mean ± s.e.m. (pooled data from $n=3$ independent experiments are shown). (**b**,**e**) *P* values were calculated using two-tailed *t*-test. (**c**,**d**) *P* values were calculated using chi-squared test. $^{***}P<0.001$; $^{****}P<0.0001$; NS, not significant.

flanked by Lac- or Tet-operator sequences at either side[20]. We chemically synthesized four 3′-fluorophore-labelled DDRNA pairs (DDRNA-Cy5) previously identified in these cells[16] (Supplementary Fig. 1A) and two control RNAs matching unrelated sequences. Localization of DDRNA-Cy5 was studied by intracellular single-molecule high-resolution localization and counting (iSHiRLoC)[21–23], following microinjection into the nucleus of NIH2/4 expressing GFP-LacR, with or without I-SceI. Strikingly, both pooled and individual pairs of microinjected DDRNAs, but not control RNAs, preferentially accumulated at the LacR spot only in cut cells, as quantified by single-molecule counting based on iSHiRLoC's stepwise photobleaching procedure[21–23] (Fig. 1a,b and Supplementary Fig. 1B–E).

Next, we investigated whether the localization of DDRNAs at the DSB is critical for their ability to activate DDR. We knocked down Dicer or Drosha to prevent endogenous DDRNA biogenesis in NIH2/4 expressing YFP-TetR and I-SceI and, following membrane permeabilization, we incubated cells with exogenous DDRNAs-Cy5 or control RNAs. While 53BP1 focus was reduced following Dicer and Drosha knockdown as expected[16], it reformed only when sequence-specific DDRNAs-Cy5 accumulated at the locus, demonstrating that

© 2017 Macmillan Publishers Limited, part of Springer Nature. All rights reserved.

site-specific localization is crucial for DDRNA ability to activate DDR (Fig. 1c and Supplementary Fig. 1F,G).

To probe the mechanisms of sequence-dependent and damage-dependent localization of DDRNAs, we knocked down H2AX to prevent DDR focus formation in NIH2/4 expressing I-SceI incubated with DDRNAs-Cy5. We observed that although 53BP1 recruitment was inhibited, DDRNAs still accumulated at the DSB (Supplementary Fig. 1H,I). To test the potential hybridization of DDRNAs to the damaged genomic site, we overexpressed RNaseH1 and this had no impact on DDRNA localization (Supplementary Fig. 1J,K). To test instead whether DDRNA localization depends on RNA–RNA base pairing with a potential nascent transcript, prior to cut induction we transiently treated NIH2/4 with α-amanitin (AM), a specific RNAPII inhibitor; 5,6-dichloro-1-β-D-ribofuranosylbenzimidazole (DRB), an inhibitor of RNAPII elongation; actinomycin D (ACTD) at a low dose to inhibit RNAPI or at a higher dose to inhibit both RNAPI and RNAPII[24]; or with vehicle alone. Specificity and efficacy of each treatment were monitored under all conditions (Supplementary Fig. 1L). Remarkably, RNAPII inhibition consistently reduced DDRNA localization to the damage site (Fig. 1d). This result was recapitulated by microinjection of DDRNA-Cy5 and I-SceI protein, with or without AM (Fig. 1e).

Together, these results indicate that DDRNAs localize to their homologous damaged site and here they stimulate DDR focus formation site-specifically, in an RNAPII-dependent manner.

Damage-induced long non-coding RNAs are generated by RNAPII and interact with DDRNA

Next, we investigated the transcriptional landscape around a DSB in search for nascent transcripts, which we named damage-induced long non-coding RNAs (dilncRNAs). I-SceI-induced DSBs in NIH2/4 cells may, in principle, generate two species of dilncRNAs at each side of the break: diverging from the DSB (*Lac-from* and *Tet-from*), and converging towards the DSB (*Lac-to* and *Tet-to*) (Fig. 2a). Single-molecule fluorescent *in situ* hybridization (smFISH[25]) with strand-specific DNA probes revealed a stronger signal at the GFP-LacR locus in cut cells than in uncut cells for divergent transcripts, and a more modest but significant increase of signal following cutting also for convergent ones (Fig. 2b and Supplementary Fig. 2A). Control probe (*Ctrl*) with an unrelated sequence did not co-localize with GFP-LacR (Fig. 2b). SmFISH signal was lost when RNaseA was added prior to hybridization or RNaseH was added after hybridization (Supplementary Fig. 2B). Careful calibration of the signal generated by probes binding only once per RNA molecule (Supplementary Fig. 2C) consistently detected an induction of dilncRNAs following cutting (Supplementary Fig. 2D).

To gain additional independent evidence, we performed strand-specific reverse transcription followed by quantitative PCR (RT–qPCR) in NIH2/4 with different sets of primers and we observed consistent dilncRNA accumulation upon damage (Fig. 2c). Reverse-transcription with oligo-dT primers did not allow dilncRNA detection, indicating that dilncRNAs lack polyadenylation (Supplementary Fig. 2E).

To determine the identity of the RNA polymerase involved, we measured dilncRNA levels by strand-specific RT–qPCR in NIH2/4 briefly treated with transcription inhibitors prior to cutting. AM, DRB or highly dosed ACTD all abolished dilncRNA induction (Supplementary Fig. 2F) and smFISH generated similar results (Supplementary Fig. 2G), indicating that damage-induced transcription is dependent on RNAPII. By contrast, ATM inhibition did not affect dilncRNA generation (Supplementary Fig. 2H).

Induction of dilncRNA was observed in several distinct cell systems: in a human cell line (U2OS19ptight[26]) bearing the same construct described for NIH2/4 (Fig. 2d) and in human and murine cell systems (HeLa111 (ref. 27) and NIH3T3duo[28]) with an integrated construct bearing the I-SceI cleavable site close to a non-repetitive sequence (Fig. 2e and Supplementary Fig. 2I).

Importantly, dilncRNAs are detectable also within endogenous genomic sites lacking any repetitive DNA sequence, such as following I-PpoI nuclease-mediated cleavage within the *DAB1* gene[29] and within an intergenic region (Fig. 2f and Supplementary Fig. 2J), following AsiSI nuclease-mediated cleavage upstream of the *CYB561D1* gene[30] and within another intergenic region (Supplementary Fig. 2K,L), and following CRISPR–Cas9-induced DNA cleavage at the *c-Myc* gene (Supplementary Fig. 2M)—in all cell systems, only the strand lacking pre-existing gene transcription was analysed.

Next, we tested whether dilncRNAs are DDRNA precursors. We knocked down Drosha or Dicer in NIH2/4 and measured the levels of dilncRNA, DDRNA and their processing intermediate species (pre-DDRNA). Strand-specific RT–qPCR revealed an accumulation of dilncRNA following Drosha knockdown in cut cells compared with siLuc control, proving that these transcripts are indeed processed by Drosha (Fig. 2g and Supplementary Fig. 2N). Since we did not detect an accumulation of dilncRNA following Dicer knockdown, we inactivated Translin, part of the Translin/Trax complex that degrades intermediate precursors of microRNA (miRNA) biogenesis in the absence of Dicer[31] and observed a rescue of dilncRNA induction in cells lacking Dicer when Translin was absent (Fig. 2g and Supplementary Fig. 2N).

To isolate DDRNA and pre-DDRNA, we purified two RNA fractions by gel extraction: a short fraction (15–40 nucleotides long) containing mature miRNA and DDRNA (Fig. 2h) and a longer fraction (40–200 nucleotides long) containing pre-miRNA and pre-DDRNA (Supplementary Fig. 2O). We observed an induction of both DDRNA and pre-DDRNA following damage; let-7a and let-7a pre-miRNA controls remained unaltered, as expected. In the absence of either Dicer or Drosha, mature DDRNA and let-7a were significantly reduced. Also, pre-DDRNA and let-7a pre-miRNA levels were reduced in the absence of Drosha and increased in the absence of Dicer (Fig. 2h and Supplementary Fig. 2O). Together, these data indicate that miRNA and DDRNA are processed similarly.

Considering that dilncRNA synthesis and DDRNA localization are RNAPII-dependent, we hypothesized that DDRNA localization and function are mediated by their interaction with dilncRNA. To test this, two different DDRNA duplexes with a 3′-end biotin modification (btn) on the strand matching *Lac-from* dilncRNA and a negative control miRNA were transfected into cut NIH2/4. By RNA pulldown assays, we observed a significant enrichment of dilncRNAs bound to DDRNAs, compared with control RNA—interactions were specific since *Rplp0* messenger RNA was not detected (Fig. 2i). These results demonstrate that sequence-dependent localization of DDRNAs relies on their pairing with dilncRNAs. The observation that dilncRNAs, like other chromatin-associated ncRNAs such as TERRA[32], are relatively

© 2017 Macmillan Publishers Limited, part of Springer Nature. All rights reserved.

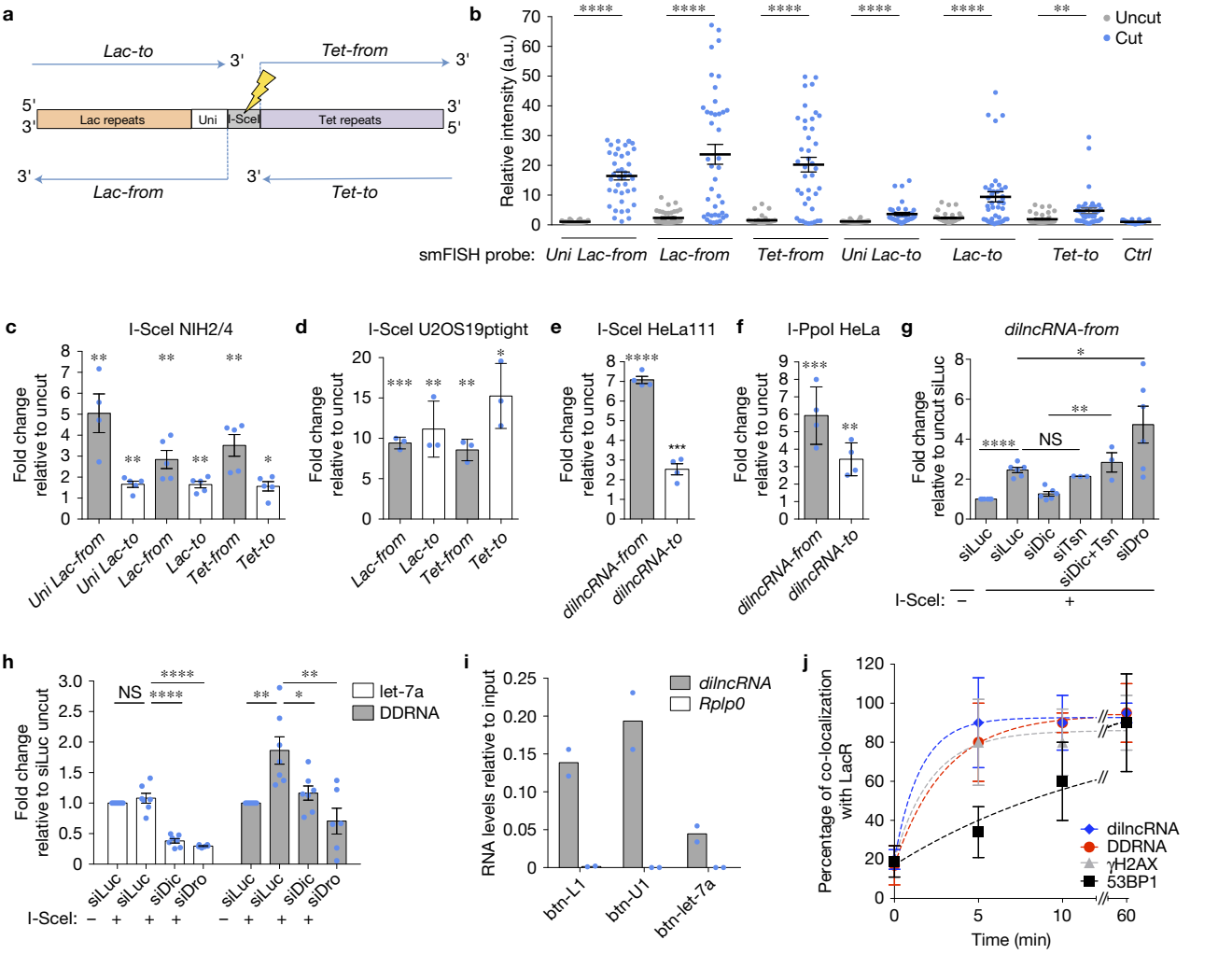

Figure 2 DSBs induce dilncRNAs that interact with DDRNAs. (**a**) Schematic of the four potential dilncRNAs induced following DSB in NIH2/4. (**b**) Induction of dilncRNAs in NIH2/4 measured by smFISH. Relative intensity of the signal generated by the indicated probes at the uncut or cut locus. The dots represent individual cells. The black bar represents the mean ± s.e.m. (data are shown as pool of $n=3$ independent experiments). (**c**–**f**) Induction of dilncRNAs in NIH2/4, U2OS19ptight, HeLa111 and I-PpoI HeLa cells measured by strand-specific RT–qPCR. The bar plots show the mean relative enrichment of the indicated RNA sets following cutting. For each RNA set, the RNA level in uncut cells was used as the normalizer. The error bars indicate s.e.m. (**c**: for *Uni Lac-from* $n=4$, for the other dilncRNAs $n=5$; **d**: $n=3$; **e**: $n=4$; **f**: $n=4$ independent experiments). (**g**) NIH2/4 cells knocked down for Drosha (siDro), Dicer (siDic), Translin (siTsn), Dicer and Translin (siDic+Tsn) or Luciferase (siLuc) were transfected with I-SceI-expressing vector (+) or empty vector (−). The bar plots show the mean relative enrichment of *Lac-from* dilncRNA relative to uncut siLuc by strand-specific RT–qPCR. The error bars indicate s.e.m. (for siLuc, siDic and siDro $n=6$, for the other conditions $n=3$ independent experiments). (**h**) NIH2/4 cells knocked down for Drosha (siDro), Dicer (siDic) or Luciferase (siLuc) were transfected with I-SceI-expressing vector (+) or empty vector (−). RNA fractions of 15–40 nt in length were recovered by gel extraction. The bar plot shows the mean relative enrichment of let-7a miRNA and DDRNAs matching Lac sequences, relative to uncut siLuc. The error bars indicate s.e.m. ($n=3$ independent experiments). (**i**) Biotinylated DDRNAs (btn-L1 and btn-U1) or biotinylated miRNA (btn-let-7a) was transfected into NIH2/4 cells expressing I-SceI and RNA pulldowns were performed. The bar plot shows dilncRNA *Lac-from* and *Rplp0* mRNA levels, assessed by strand-specific RT–qPCR, as relative to input. Values are expressed as the mean of two independent experiments. (**j**) Time course of γH2AX and 53BP1 focal accumulation by immunofluorescence, dilncRNA generation by smFISH and fluorescent DDRNA localization at the DSB in NIH2/4. The plot shows the percentage of cells bearing signals co-localizing with LacR. The dashed line represents the best fit of the data to a single exponential function. The error bars indicate s.d. ($n=3$ independent experiments, ≥12 cells analysed in total per time point). *P* values were calculated using two-tailed *t*-test. $^{*}P<0.05$; $^{**}P<0.01$; $^{***}P<0.001$; $^{****}P<0.0001$; NS, not significant. Statistical source data are provided in Supplementary Table 4.

resistant to RNaseA treatment (Supplementary Fig. 2P,Q) helps explain our reported activity of exogenously added DDRNAs in DDR foci reformation in RNaseA-treated cells[16].

We next performed a time course study of the individual events following DSB induction. In parallel to the expected fast γH2AX accumulation, dilncRNA generation and DDRNA localization to the LacR spot were detectable as early as 5 min after damage induction and increased with very similar kinetics (Fig. 2j). 53BP1 accumulation was tenfold slower. These observations suggest that dilncRNA induction and DDRNA localization to the damaged site are upstream signals that, together with γH2AX, nucleate DDR focus formation.

© 2017 Macmillan Publishers Limited, part of Springer Nature. All rights reserved.

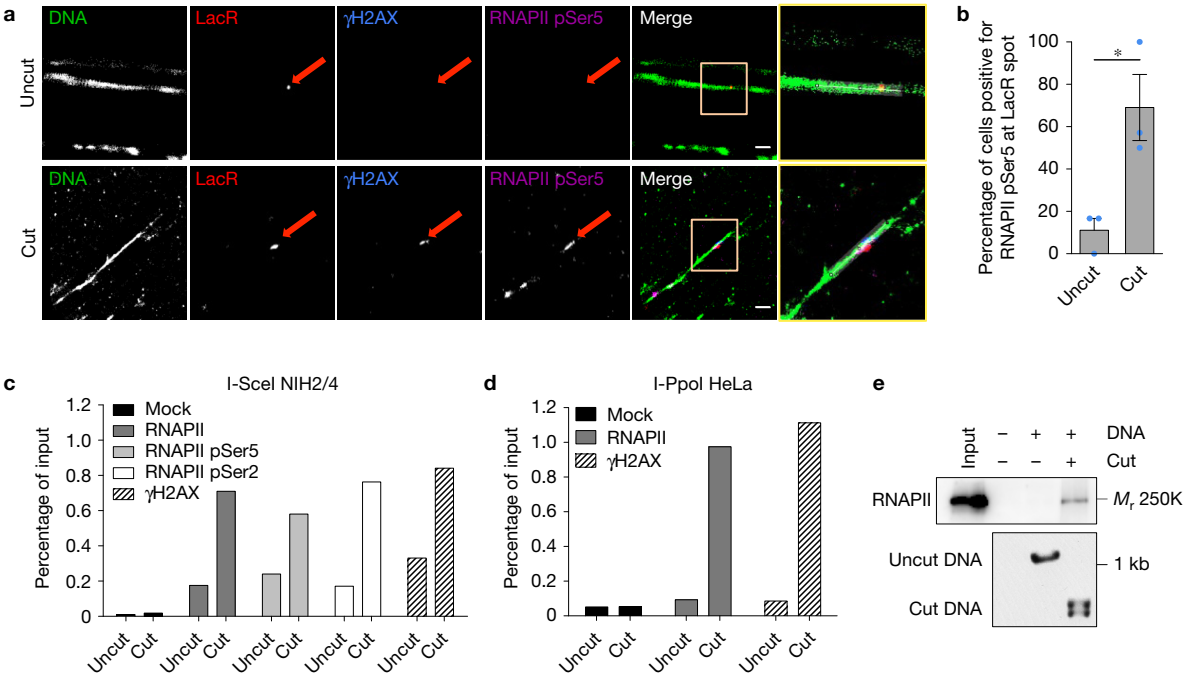

Figure 3 Active RNAPII is recruited to DSBs in mammalian cells and in cell extracts. (**a**) Detection of γH2AX and RNAPII pSer5 at the DNA damage locus on chromatin spreads by super-resolution microscopy. Representative super-resolution images of chromatin fibres (green), LacR (red), γH2AX (blue) and RNAPII pSer5 (purple) in uncut and cut NIH2/4 cells. The yellow-outlined images correspond to the yellow-outlined inset region. Scale bar, 500 nm. (**b**) The bar plot is the quantification of **a** and represents the percentage of cells showing γH2AX and active RNAPII pSer5 co-localizing with LacR by super-resolution microscopy on chromatin spreads in uncut and cut conditions. Data are shown as mean. The error bars indicate s.e.m. ($n=3$ independent experiments, ≥20 images per sample per experiment). (**c**) Accumulation of RNAPII at the damaged locus by ChIP in uncut and cut NIH2/4 cells. The bar plot shows the percentage of enrichment relative to the input of RNAPII, RNAPII pSer5 and RNAPII pSer2 associated with genomic DNA, as detected with primers matching Lac sequences flanking the I-SceI-induced DSB. Data are shown as one representative of three independent experiments. (**d**) The bar plot shows the percentage of enrichment relative to the input of γH2AX and total RNAPII at the endogenous *DAB1* locus by ChIP in HeLa cells cut by I-PpoI. Data are shown as one representative of three independent experiments. (**e**) Biotinylated DNA immobilized on streptavidin beads was either cut or not cut by recombinant I-SceI enzyme *in vitro* and incubated with nuclear cell extract. Input and pulldown samples were probed for total RNAPII. Below, an agarose gel shows equal amounts of uncut or cut DNA employed. This experiment was repeated three times independently with similar results. *P* value was calculated using two-tailed *t*-test. $^{*}P<0.05$. Statistical source data are provided in Supplementary Table 4. Unprocessed original scans of blots are shown in Supplementary Fig. 9.

Active RNAPII is recruited to DSB

We next sought evidence for accumulation of RNAPII at DSBs. We isolated NIH2/4 nuclei from cut or uncut cells expressing Cherry-LacR and analysed by confocal microscopy γH2AX and transcribing RNAPII (RNAPII pSer5) (Supplementary Fig. 3A). RNAPII pSer5 was significantly enriched at the cut locus (Supplementary Fig. 3B) and correlated with γH2AX presence (Supplementary Fig. 3C,D). By imaging chromatin fibres with super-resolution binding-activatable localization microscopy (BALM)[33], we detected a co-localization of RNAPII pSer5 with the LacR spot (Fig. 3a,b and Supplementary Fig. 3E). Furthermore, chromatin immunoprecipitation (ChIP) analyses in NIH2/4 revealed that total RNAPII, RNAPII pSer5 and RNAPII pSer2 were enriched following DSB induction, similarly to γH2AX (Fig. 3c and Supplementary Fig. 3F). As controls, both total and phosphorylated forms of RNAPII were absent in intergenic regions and present in coding and promoter-proximal regions of the β-actin gene (Supplementary Fig. 3G–I). RNAPII accumulation was detected by ChIP also at an endogenous locus cut by I-PpoI in HeLa cells (Fig. 3d and Supplementary Fig. 3J).

To test whether the RNAPII complex has the ability to recognize DNA double-stranded ends, a biotinylated DNA fragment was immobilized on streptavidin beads in its intact form or cut by I-SceI, and incubated with nuclear extracts. We observed total and phosphorylated RNAPII associated only with DNA bearing free ends (Fig. 3e and Supplementary Fig. 3K).

Taken together, these results indicate that transcribing RNAPII can be detected at DSBs by imaging and ChIP and that it has an affinity for double-stranded DNA ends.

DSBs induce bidirectional transcription by RNAPII in cell-free extracts

Next, we characterized dilncRNA synthesis in transcription-competent human cell extracts containing a plasmid bearing an I-SceI recognition site and [α-^{32}P]UTP. Consistent with the lack of eukaryotic transcriptional promoters in the plasmid, no discrete products were detected when the circular plasmid was incubated with cell extracts (Fig. 4a and Supplementary Fig. 4A–C). By contrast, discrete products were detected when a DSB was introduced by recombinant I-SceI. Similar results were obtained with other plasmids linearized with various restriction enzymes, generating DNA ends of different sequence and structure (Supplementary Fig. 4D–F). The observed products were DNaseI resistant, RNaseA sensitive (Fig. 4a)

© 2017 Macmillan Publishers Limited, part of Springer Nature. All rights reserved.

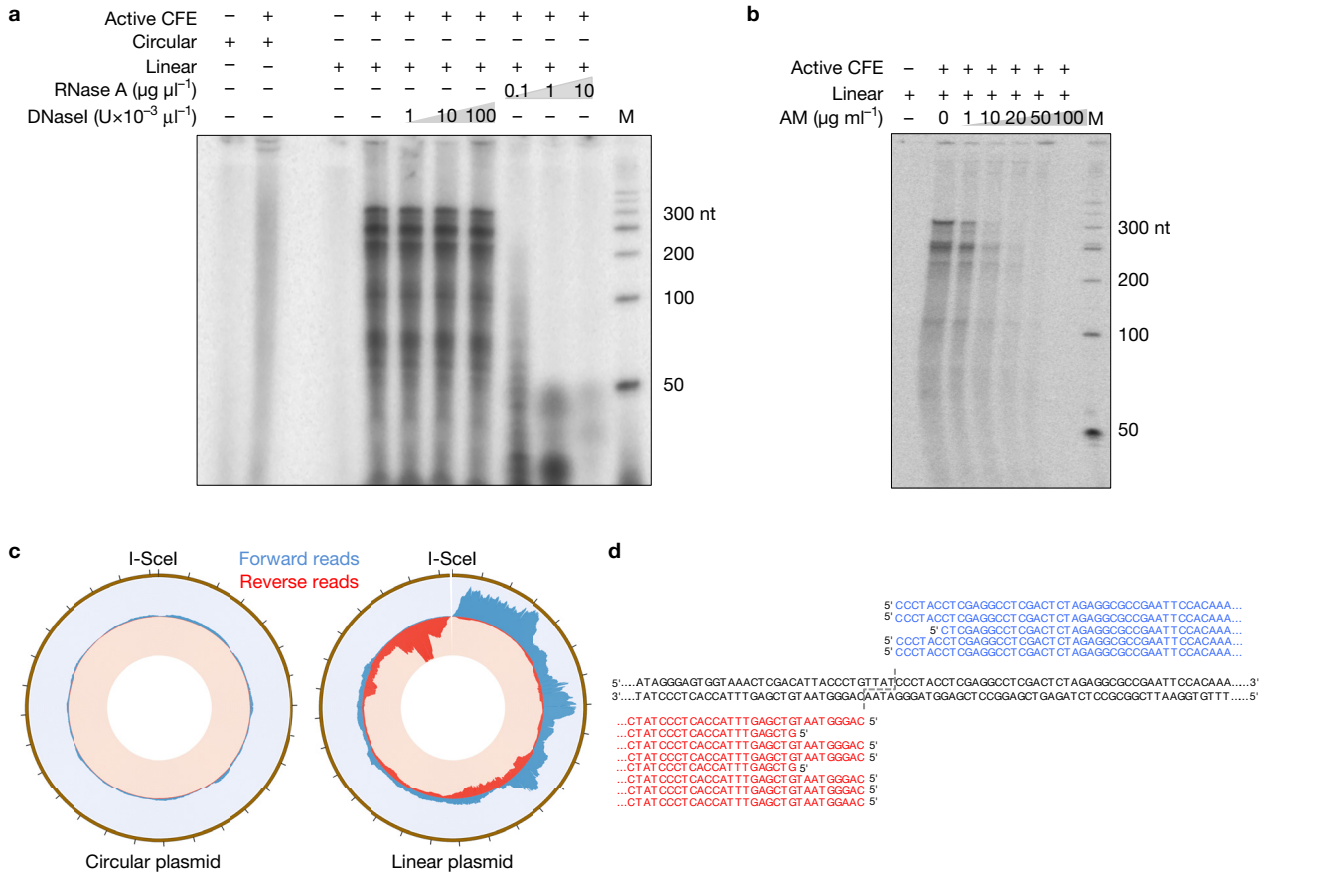

Figure 4 DSBs induce bidirectional transcription in cell-free extracts. (**a**) Transcriptionally competent human cell-free extracts (CFE; '+' and '−' indicate active or heat-inactivated CFE, respectively) were incubated with a circular or I-SceI-linearized form of the pLac-Tet plasmid in the presence of [α-^{32}P]UTP. Where indicated, products were treated with increasing amounts of DNaseI or RNaseA. Products were resolved on a denaturing PAGE, along with a radiolabelled DNA ladder (M, nt indicates nucleotides). This experiment was repeated three times independently with similar results. (**b**) In the same settings described in **a**, AM reduces DSB-induced transcription. This experiment was repeated three times independently with similar results. (**c**) An ion proton sequencer was used to perform deep sequencing of the RNA products generated in **a**. From the outer to the inner circles, the plots display the entire plasmid (brown, 2,834 bp with ticks showing 100 bp intervals), and the coverage of forward reads (blue, maximum value of the distribution is set to 1,300) and reverse reads (red, maximum value of the distribution is set to 8,000) for each nucleotide position of both circular and linearized plasmids. (**d**) Individual 5′ RACE clones (in blue forward, in red reverse) are aligned to the sequence of the DNA substrate used. The site of DSB generation is indicated by the dashed line. Unprocessed original scans of radioactive blots are shown in Supplementary Fig. 9.

and their production was prevented by the RNAPII inhibitor AM (Fig. 4b). Also in this system, dilncRNA generation was independent from ATM (Supplementary Fig. 4G,H) and other PI(3)K-like kinases (Supplementary Fig. 4I–L).

Deep sequencing of these RNA products showed a clear pattern of robust divergent bidirectional RNA synthesis originating from the DSB (Fig. 4c). Mapping of the transcription start site by 5′ rapid amplification of complementary DNA ends (5′ RACE) indicated that transcription starts at or within a few nucleotides from the DNA end (Fig. 4d). Thus, also in a cell-free system, DSBs trigger the bidirectional synthesis of RNAPII-dependent transcripts originating from the DSB.

MRN and RNAPII interact following DNA damage in mammalian cells

The MRN complex is a primary sensor of DSBs and thus a plausible mediator of RNAPII activity at DSBs. To investigate the potential interaction between MRN and RNAPII, we individually immunoprecipitated the three subunits of the MRN complex from untreated or irradiated cells and probed for RNAPII and its phosphorylated forms. Both total and phosphorylated RNAPII were robustly detected interacting with MRN in extracts from irradiated cells (Fig. 5a).

When we knocked down MRN in NIH2/4, we observed a reduction of dilncRNA induction following I-SceI cutting (Fig. 5b and Supplementary Fig. 5A). Similar results were obtained by RT–qPCR and smFISH with the MRN inhibitor mirin[34] (Fig. 5c,d). Impaired dilncRNA synthesis in the absence of a functional MRN was the consequence of a reduced RNAPII association with DSBs as demonstrated by ChIP experiments (Fig. 5e) and imaging (Supplementary Fig. 5B,C).

Taken together, these results show that MRN interacts with RNAPII following DNA damage and suggest a role for MRN in RNAPII recruitment and activity at DSBs.

RNAPII activity is necessary for DDR focus formation and DNA repair and 53BP1 interacts with DDRNA and dilncRNA

We next sought evidence for a role of RNAPII activity in DDR regulation in living cells. We discovered that acute RNAPII

© 2017 Macmillan Publishers Limited, part of Springer Nature. All rights reserved.

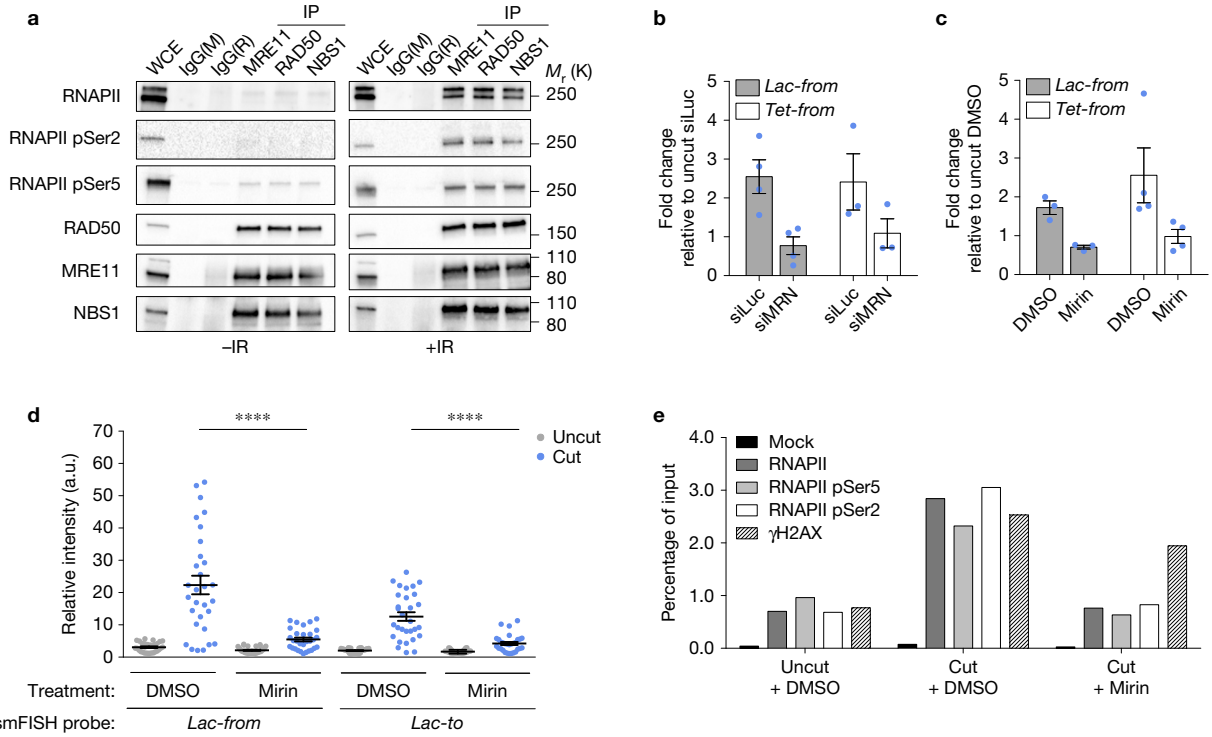

Figure 5 The MRN complex binds to RNAPII following DNA damage and is necessary for RNAPII transcription at DSBs in mammalian cells. (**a**) Co-immunoprecipitation of RNAPII and its phosphorylated forms with the MRN complex following IR exposure. HEK293Tcells were irradiated (+IR) or not (−IR) and samples were collected 10 min post IR, followed by immunoprecipitation of the individual components of the MRN complex. Whole-cell extract (WCE) and immunoprecipitated samples were analysed by immunoblotting. Mouse (IgG(M)) or rabbit (IgG(R)) immunoglobulins were used as a control. This experiment was repeated twice independently with similar results. (**b**) DSB-induced transcription is dependent on MRN. The bar plot shows the mean relative enrichment of the indicated RNA sets by strand-specific RT–qPCR in cut NIH2/4 cells knocked down for the three components of the MRN complex (siMRN) or in siLuciferase (siLuc)-transfected cells as a control. For each RNA set, the RNA level in uncut cells was used as the normalizer. The error bars indicate s.e.m. (for *Lac-from* $n=4$, for *Tet-from* $n=3$ independent experiments). (**c**) DSB-induced transcription is reduced by the MRN inhibitor mirin. The bar plot shows the mean relative enrichment of the indicated RNA sets by strand-specific RT–qPCR in NIH2/4 cell treated with mirin or dimethylsulfoxide (DMSO) as a control 2 h before cut induction. For each RNA set, the RNA level in uncut cells was used as the normalizer. The error bars indicate s.e.m. (for *Lac-from* $n=3$, for *Tet-from* $n=4$ independent experiments). (**d**) Relative intensity of the signal generated by the indicated smFISH probes at the uncut or cut locus, in DMSO- or mirin-treated samples. The dots represent individual cells. The black bar represents the mean ± s.e.m. (pooled data from $n=3$ independent experiments are shown). (**e**) Accumulation of active RNAPII at the damaged locus by ChIP in cut NIH2/4 cells is reduced by mirin. The bar plot shows the percentage of enrichment relative to the input of total RNAPII, RNAPII pSer5 and RNAPII pSer2 associated with genomic DNA as detected by primers matching Lac sequences flanking the I-SceI-induced DSB. Data are shown as one representative of two independent experiments. *P* values were calculated using two-tailed *t*-test. $^{****}P<0.0001$. Statistical source data are provided in Supplementary Table 4. Unprocessed original scans of blots are shown in Supplementary Fig. 9.

inhibition, as achieved by AM, DRB, or ACTD at high doses, prevented DDR activation in the form of 53BP1 and pATM foci at the LacR spot, without affecting γH2AX signals (Fig. 6a–c and Supplementary Fig. 5D–I). High-resolution imaging in NIH2/4 microinjected with I-SceI together with AM revealed that RNAPII inhibition abolished nucleation and growth of 53BP1 focus over time (Supplementary Fig. 5J).

RNAPII inhibition also impaired 53BP1 and pATM focus formation induced by ionizing radiation, thus at several different endogenous genomic loci, in HeLa cells and human normal fibroblasts (BJ) (Fig. 6d–f and Supplementary Fig. 6A–L). These brief treatments did not affect *53BP1* and *ATM* mRNA levels in all cell lines used (Supplementary Figs 5G,I and 6E,G,J). ChIP–qPCR experiments in BJ cells expressing AsiSI-ER confirmed impaired 53BP1 accumulation on damaged chromatin in DRB-treated cells, at DSBs generated within or outside a transcriptional unit (genic and intergenic AsiSI, respectively; Supplementary Fig. 7A–F); as expected, γH2AX remained unaffected. RNAPII inhibition also reduced foci of RIF1 (ref. 35), pKAP1 (ref. 36), RNF168 (ref. 37) and irradiation-induced conjugated ubiquitin signals (Supplementary Fig. 7G–J).

To test the impact of RNAPII inhibition on DNA repair following irradiation, we employed two complementary approaches in different cell lines (BJ and HeLa cells): persistence of γH2AX foci detected by immunfluorescence and the neutral comet assay. We observed impaired DNA repair in DRB-treated cells in comparison with control dimethylsulfoxide (DMSO)-treated cells, as indicated by the prolonged persistence of γH2AX foci (Fig. 6g and Supplementary Fig. 8A), as well as by the increased tail moment (Fig. 6h,i and Supplementary Fig. 8B).

53BP1 has been reported to interact with RNA in a manner dependent on its Tudor domain[38]. We therefore tested by RNA immunoprecipitation assays the ability of 53BP1 to bind to ncRNAs generated at damaged sites. We observed that endogenous DDRNAs and dilncRNAs bind to 53BP1 in NIH2/4 cells expressing I-SceI and

© 2017 Macmillan Publishers Limited, part of Springer Nature. All rights reserved.

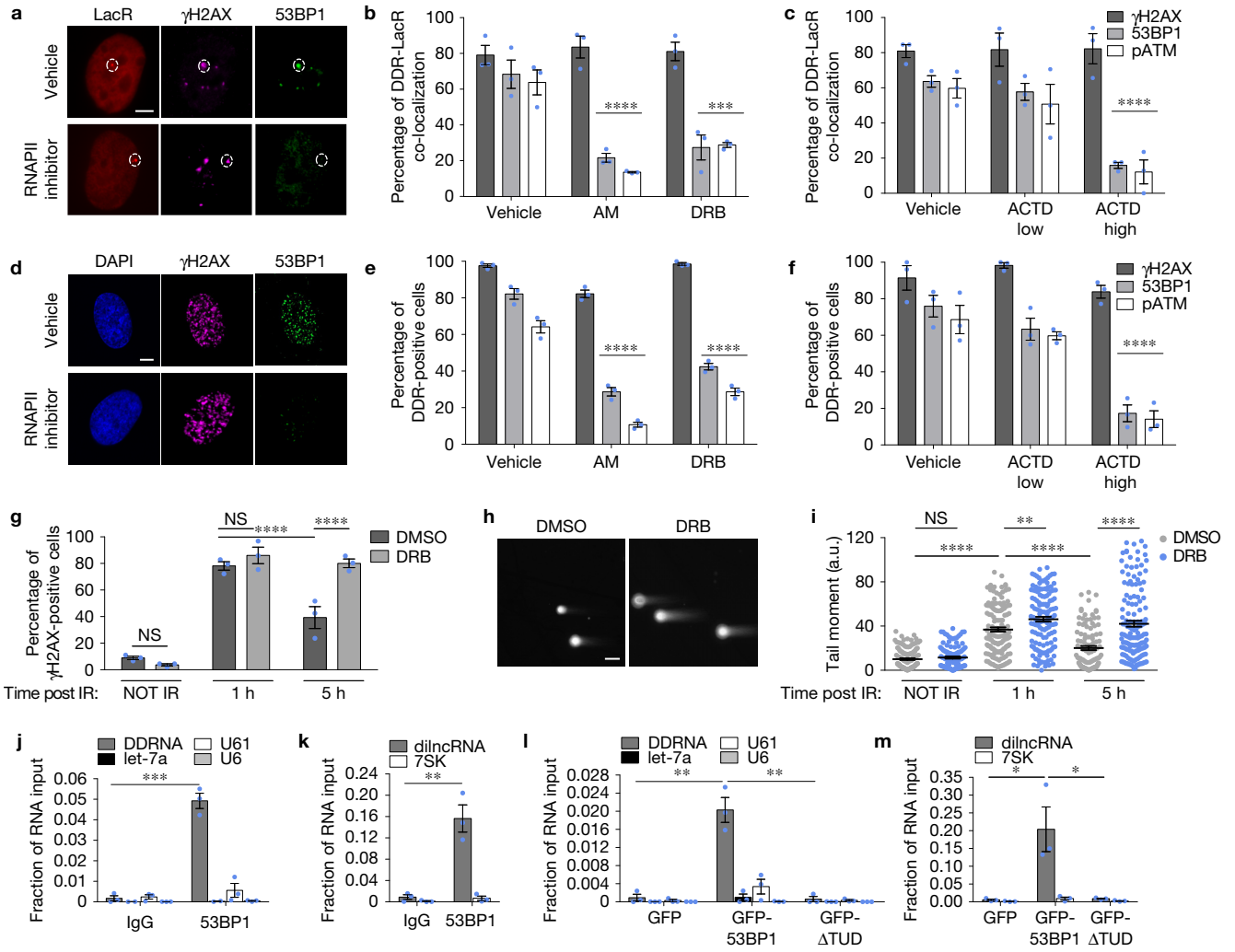

Figure 6 RNAPII transcription is necessary for DDR focus formation and DNA repair, and 53BP1 interacts with DDRNA and dilncRNA through its Tudor domain. (**a**) NIH2/4 cells treated with vehicle or an RNAPII inhibitor (AM in these images) before cut induction. Scale bar, 5 μm. (**b**,**c**) Quantification of **a** showing the percentage of cells positive for DDR markers co-localizing with LacR in NIH2/4 cells treated with AM, DRB, ACTD or vehicle for 2 h before cut induction. The error bars indicate s.e.m. ($n=3$ independent experiments, ≥70 cells analysed in total per condition). (**d**) Representative images of human normal fibroblasts (BJ) treated with vehicle or an RNAPII inhibitor (DRB in these images) before IR. Scale bar, 5 μm. Quantification is shown in Supplementary Fig. 6L. (**e**,**f**) Percentage of DDR-positive HeLa cells treated with AM, DRB, ACTD or vehicle before IR (cells with >10 foci were considered positive). The error bars indicate s.e.m. ($n=3$ independent experiments, ≥200 cells analysed in total per condition). (**g**) The bar plot shows the percentage of γH2AX-positive BJ cells pre-treated with DMSO or DRB for 2 h, irradiated (2 Gy) and fixed at the indicated time points (irradiated cells with >30 foci were considered positive). The error bars indicate s.e.m. ($n=3$ independent experiments, ≥200 cells analysed in total per condition). (**h**) Representative images of a neutral comet assay at 5 h post irradiation. Scale bar, 5 μm. Quantification is shown in **i**. (**i**) The scatter plot shows the tail moment analysis of the neutral comet assay of HeLa cells pre-treated with DMSO or DRB for 2 h, irradiated (5 Gy) and collected at the indicated time points. The dots represent individual cells. The black bars indicate the mean. The error bars indicate s.e.m. (pooled data from $n=3$ independent experiments are shown, ≥100 tails analysed in total per condition). (**j**,**k**) Endogenous 53BP1 was immunoprecipitated in cut NIH2/4 cells and RNA bound to it was analysed by small RNA-specific RT–qPCR or strand-specific RT–qPCR. The results are shown as the mean fraction of input. The error bars indicate s.e.m. ($n=3$ independent experiments). (**l**,**m**) Constructs expressing GFP, GFP-53BP1 or GFP-53BP1 lacking the Tudor domain (GFP-53BP1ΔTUD) were transfected in NIH2/4 cells expressing I-SceI. Immunoprecipitation with anti-GFP antibody and RNA analysis was performed as in **l**. The results are shown as the mean fraction of input. The error bars indicate s.e.m. ($n=3$ independent experiments). (**b**–**g**) *P* values were calculated using chi-squared test. (**i**–**m**) *P* values were calculated using two-tailed *t*-test. $^{*}P<0.05$; $^{**}P<0.01$; $^{***}P<0.001$; $^{****}P<0.0001$; NS, not significant. Images in **a**,**d**,**h** are representative of three independent experiments. Statistical source data are provided in Supplementary Table 4.

that this binding is specific, since other abundant nuclear small RNAs were not enriched (Fig. 6j,k). To test the role of the Tudor domain, we transfected a GFP-tagged version of the minimal portion of 53BP1 (1220-1631) reportedly sufficient to drive its localization to DNA damage foci[39], or the same portion deleted for the Tudor domain (ΔTUD). We observed that this GFP-53BP1 minimal construct interacts with both DDRNAs and dilncRNAs in a specific manner and that the deletion of the Tudor domain completely abolishes such interactions (Fig. 6l,m).

Collectively, our results demonstrate that RNAPII transcription is necessary for DDR focus formation and DNA repair and that 53BP1 associates with DDRNA and dilncRNA.

© 2017 Macmillan Publishers Limited, part of Springer Nature. All rights reserved.

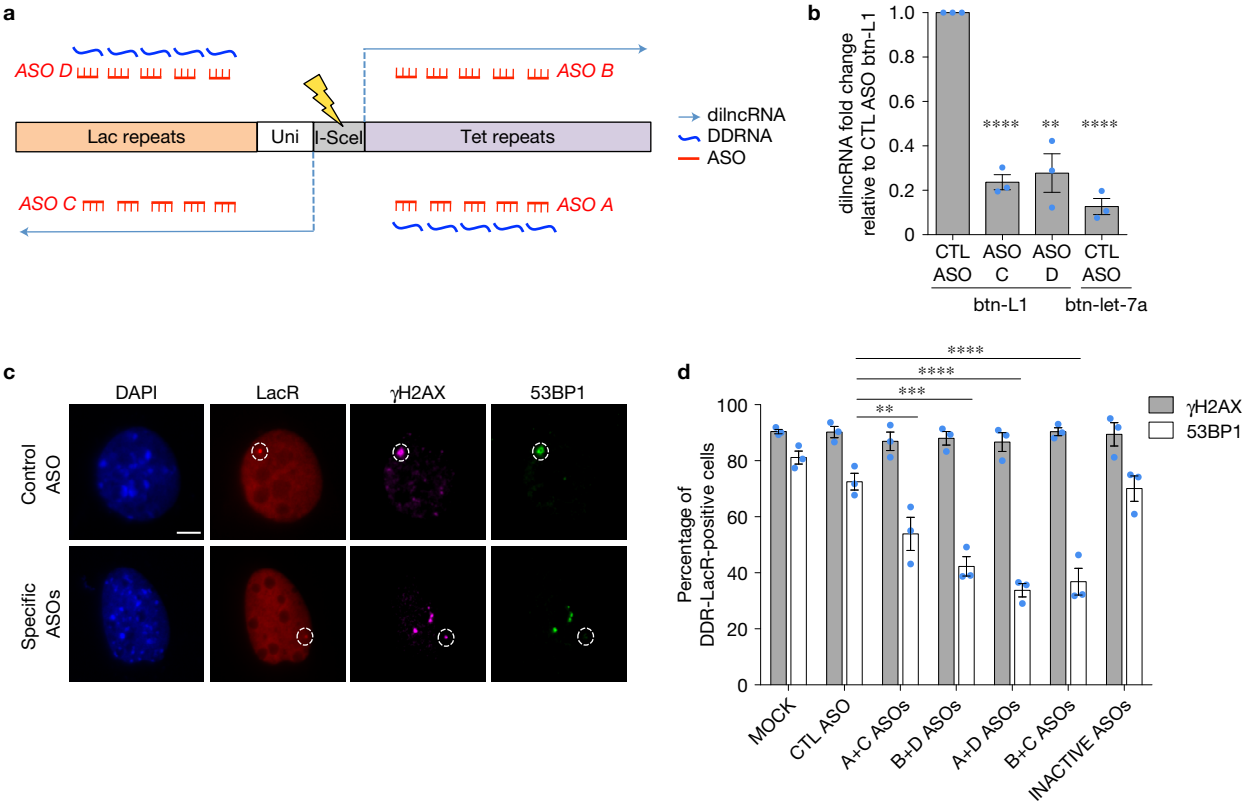

Figure 7 ASOs preventing dilncRNA–DDRNA interaction affect 53BP1 focus formation. (**a**) Schematic representation of ASOs (red) preventing the interaction between dilncRNAs (light blue) and DDRNAs (dark blue), originating from Lac or Tet sequences flanking the I-SceI site in NIH2/4 cells. For clarity, *dilncRNA-from*, but not *dilncRNA-to*, and the corresponding complementary DDRNA are shown. (**b**) NIH2/4 cells expressing I-SceI were transfected with control ASO (CTL) or specific ASOs matching Lac sequences (ASOs C, D) and subsequently with biotinylated DDRNA (btn-L1) or a biotinylated miRNA (btn-let-7a). After cut induction, RNA pulldown was performed. The bar plot shows the fold change of dilncRNA (*Lac-from*) levels, assessed by strand-specific RT–qPCR as relative to input, with respect to control levels (CTL ASO + btn-L1). The values are expressed as the mean. The error bars indicate s.e.m. ($n=3$ independent experiments). (**c**) Representative images of cut NIH2/4 cells transfected with control or specific ASOs and probed for γH2AX and 53BP1. The white circles mark the LacR spot. Scale bar, 5 μm. (**d**) The bar plot shows the quantification of **c** and shows the percentage of cut NIH2/4 cells positive for LacR co-localization with γH2AX and 53BP1 in the presence of different sets of ASOs. ASO with a sequence unrelated to the locus (CTL) or pre-annealed (INACTIVE) ASOs were used as control. The error bars indicate s.e.m. ($n=3$ independent experiments, ≥100 cells analysed in total per condition). (**b**) *P* values were calculated using two-tailed *t*-test. (**d**) *P* values were calculated using chi-squared test. $^{**}P<0.01$; $^{***}P<0.001$; $^{****}P<0.0001$; NS, not significant. Statistical source data are provided in Supplementary Table 4.

Sequence-specific DDR and DNA repair inhibition by antisense oligonucleotides

Given the evidence of sequence-specific pairing between DDRNAs and dilncRNAs, we reasoned that DDR activation could be inhibited at individual genomic sites by the use of sequence-specific antisense oligonucleotides (ASOs), blocking DDRNA–dilncRNA interaction. We therefore designed four ASOs against dilncRNAs and DDRNAs containing Lac or Tet sequences (Fig. 7a) or a control. To demonstrate that ASOs indeed disrupt DDRNA–dilncRNA interactions, NIH2/4 expressing I-SceI were transfected with individual ASOs against Lac sequences or a control ASO prior to transfection of biotinylated DDRNA or let-7a as a control. By RNA pulldown assay performed as in Fig. 2i, we observed that DDRNA–dilncRNA interactions were significantly reduced by sequence-specific ASOs (Fig. 7b).

Then, to study DDR, four different combinations of two ASOs were transfected into cut NIH2/4 to inhibit RNAs originating from both sides of the DSB. Remarkably, 53BP1 accumulation at the locus was significantly reduced following transfection of all sequence-specific ASOs tested, compared with control ASOs or mock transfection, while γH2AX was still present (Fig. 7c,d and Supplementary Fig. 8C). Transfection of ASO–ASO complementary duplexes, thus with no RNA-binding potential, did not alter 53BP1 focus formation (Fig. 7d and Supplementary Fig. 8C). Irradiation-induced DDR foci were unaffected by ASOs in the same cells (Supplementary Fig. 8D).

We next aimed to selectively inhibit DDR at a specific damaged genomic locus, while leaving DDR activity unperturbed at other damaged sites within the same nucleus. To this end, we used NIH3T3duo cells[28], bearing Lac-I-SceI and Tet-I-SceI-Tet loci integrated in different genomic sites and expressing GFP-LacR and Cherry-TetR. Co-transfection of I-SceI-expressing vector with two individual ASOs matching only Tet sequences (Supplementary Fig. 8E) or a control ASO did not significantly affect γH2AX foci at both Tet-containing and Lac-containing cut loci (Fig. 8a,b). Strikingly, the two Tet-specific ASOs impaired DDR activation, as monitored by 53BP1 focus formation, only at Tet loci, while leaving DDR activation at Lac sites within the same nucleus unaffected (Fig. 8a,b).

© 2017 Macmillan Publishers Limited, part of Springer Nature. All rights reserved.

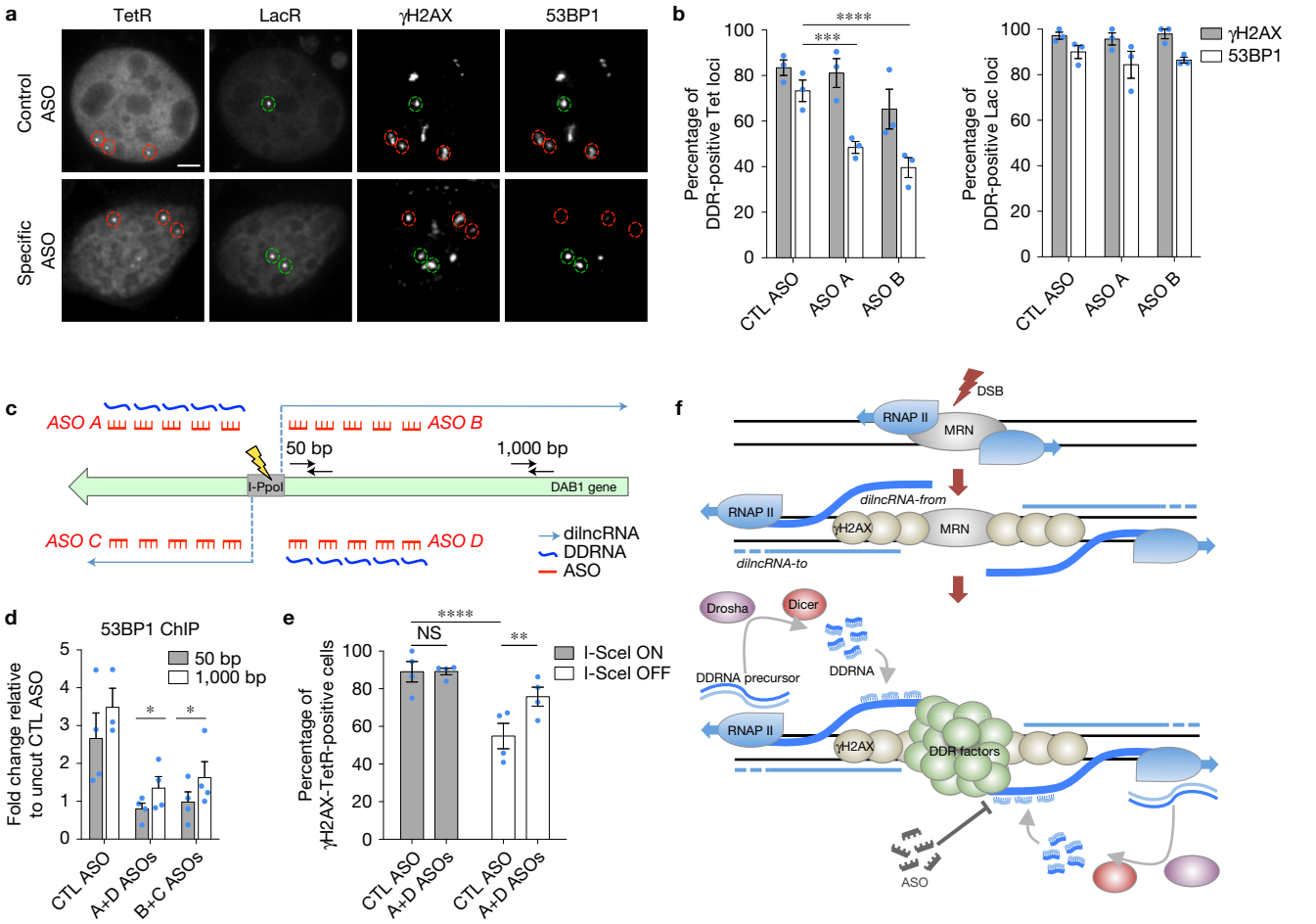

Figure 8 Site-specific inhibition of 53BP1 focus formation and DNA repair by ASOs. (**a**) Representative images of cut NIH3T3duo cells transfected with control or Tet-specific ASOs and probed for γH2AX and 53BP1. The red circles mark TetR dots; the green circles mark LacR dots. Scale bar, 5 μm. (**b**) The bar plots are the quantification of **a** and show the percentage of TetR or LacR co-localization with γH2AX and 53BP1 in the presence of control (CTL) or Tet-specific ASOs. The error bars indicate s.e.m. ($n=3$ independent experiments, ≥150 Tet loci and ≥70 Lac loci analysed in total per condition). (**c**) Schematic representation of the sets of ASOs (red) preventing the interaction between dilncRNAs (light blue) and DDRNAs (dark blue) originating from the DSB in the *DAB1* locus in HeLa cells cut by I-PpoI, and primers used for RT–qPCR (black). For clarity, *dilncRNA-from*, but not *dilncRNA-to*, and the corresponding complementary DDRNA are shown. (**d**) HeLa cells expressing inducible I-PpoI were transfected with control (CTL ASO) or specific ASOs targeting RNA molecules originated from the DSB within the endogenous *DAB1* locus. The bar plot shows the mean fold change normalized to uncut CTL ASO of enrichment relative to input of 53BP1 at the *DAB1* locus at 50 and 1,000 bp from the DSB. The error bars indicate s.e.m. ($n=3$ independent experiments). (**e**) NIH2/4 cells expressing inducible I-SceI were transfected with specific ASOs or CTL ASO. I-SceI ON: 3 h after induction, I-SceI OFF: 24 h after removal of inducing agent. The bar plot shows the percentage of cells positive for γH2AX-TetR co-localization. The error bars indicate s.e.m. ($n=4$ independent experiments, ≥80 cells analysed in total per condition). (**f**) MRN recruits RNAPII at the DSB triggering the bidirectional synthesis of *dilncRNA-from* (blue) and, in general less abundantly, of *dilncRNA-to* (light blue). DROSHA and DICER process the long double-stranded RNA, probably the outcome of paired or folded dilncRNAs, generating DDRNAs that pair with nascent unprocessed single-stranded dilncRNAs; together they bind to 53BP1 and fuel DDR focus formation. Interfering with dilncRNA–DDRNA interactions through ASOs allows site-specific inhibition of DDR. (**b**,**e**) *P* values were calculated using chi-squared test. (**d**) *P* values were calculated using two-tailed *t*-test. $^{*}P<0.05$, $^{**}P<0.01$; $^{***}P<0.001$, $^{****}P<0.0001$. Statistical source data are provided in Supplementary Table 4.

To extend these conclusions to endogenous sites, we transfected ASOs targeting DDRNAs and dilncRNAs originating from a DSB generated by I-PpoI in HeLa cells (Fig. 8c) in two different combinations. ChIP–qPCR demonstrated that 53BP1 enrichment was significantly reduced near the DSB (50 bp) and away from it (1,000 bp) following transfection of both sets of sequence-specific ASOs, compared with control ASO, while γH2AX accumulation was not (Fig. 8d and Supplementary Fig. 8F,G). 53BP1 enrichment at a different I-PpoI cut site[29] was not affected by these ASOs (Supplementary Fig. 8H) and an unrelated genomic locus on chromosome 22 not cut by I-PpoI remained unperturbed (Supplementary Fig. 8I), confirming the sequence-specificity of the treatments.

Finally, to support a direct role of dilncRNA and DDRNA in DSB repair, we transfected NIH2/4 expressing inducible I-SceI with control ASO or sequence-specific ASOs (as in Fig. 7d). After cut induction (I-SceI ON), the inducing agent was removed and DNA repair was allowed for 24 h (I-SceI OFF). By monitoring γH2AX persistence at the I-SceI cut locus, we observed that ASOs targeting DDRNAs and dilncRNAs at the locus indeed impaired DNA repair in a sequence-dependent manner (Fig. 8e).

© 2017 Macmillan Publishers Limited, part of Springer Nature. All rights reserved.

Our results demonstrate that it is possible to modulate DDR activation and DNA repair in a sequence-specific manner by inhibiting the RNA species generated at a damaged locus, without affecting ongoing DDR signalling at other damaged sites even within the same cell.

DISCUSSION

According to the current model, each DDR focus in a cell nucleus is similar in composition to any other one, sharing a largely overlapping set of DDR protein factors. No components have so far been demonstrated to individually mark DDR events at distinct genomic loci. Here we have shown that each DDR focus, while composed of a common set of shared proteins, also hosts a unique set of ncRNA molecules generated *in situ*, essential for DDR focus formation. Our results are consistent with a model in which DSBs trigger the generation of dilncRNAs divergent from and convergent to DNA ends, with the potential to form a double-stranded RNA that is processed by DROSHA and DICER to generate DDRNAs (Fig. 8f). Indeed, mammalian DICER has recently been reported to be phosphorylated following DNA damage and to associate with DSBs[40]. DDRNAs localize to the damaged locus through base-pairing with unprocessed dilncRNAs emerging from the DSB and concur to activate DDR (Fig. 8f). These events are reminiscent of those at the centromeric locus in *Schizosaccharomyces pombe*, where small RNAs generated by Dicer bind to a nascent transcript that is also their precursor and together maintain the epigenetic and genetic stability of the locus[41]. The proposed model fits with the growing list of small ncRNAs interacting with and regulating long ncRNAs[42] and, more in general, with the emerging interplay between DSB and transcriptional control[43].

Our observations indicate that DNA ends act as transcriptional promoters, regardless of the genomic location. Indeed, dilncRNAs can be generated within canonical genes as well as in intergenic regions. Transcription induced from the DSB is more robust and, at present, better mechanistically understood than transcription to the DSB; the latter may be the outcome of a generally more permissive environment for transcription at the DNA end, the result of unconventional RNAPII activities or consequent to dilncRNA-from transcription termination[44,45].

Several reports, including ours, have shown that DSBs can suppress gene expression[46,47]. Nonetheless, RNAPII has been detected within γH2AX domains[30,47], it can accumulate on damaged chromatin[48] and binds to some DNA repair factors[12]. A recent report on the engagement of yeast RNAPII at DSBs further supports our conclusions[11]. Thus, silencing of canonical coding transcription and concomitant *de novo* induction of non-coding RNA may coexist at damaged sites.

The ability of the MRN complex to sense the DSB, interact with RNAPII and stimulate transcription from DNA ends fits nicely with its apical role in DDR activation. Interestingly, RNAPII binding to MRN components following DNA damage has been independently observed in a proteomic screen[49]. Further studies are needed to understand the exact mechanism of MRN and RNAPII interaction, including their potential reciprocal crosstalk and the contribution of other DDR factors.

The observation that 53BP1 associates with DDRNAs and dilncRNAs in a manner dependent on its Tudor domain suggests that one of the mechanisms of recruitment to DSBs of 53BP1, and potentially of other DDR factors, is its ability to interact with *in situ*-generated DDRNAs and dilncRNAs. However, whether this interaction is direct or mediated by other factors is unknown. Inhibition by sequence-specific ASOs of 53BP1 localization to damaged chromatin and spreading is in line with the role of DICER- and DROSHA-dependent RNA products in DDR activation, as reported by us and others[7,16–18,40,50].

Finally, our data using RNAPII inhibitors and ASOs indicate that damage-induced transcription is one of the earliest events following DSB generation, concurring, together with γH2AX, to nucleate DDR focus formation. We propose that the ability to modulate DDR and DNA repair with ASOs in a sequence-specific manner may represent a new experimental tool, as well as an attractive therapeutic approach. □

METHODS

Methods, including statements of data availability and any associated accession codes and references, are available in the online version of this paper.

Note: Supplementary Information is available in the online version of the paper

ACKNOWLEDGEMENTS

We thank E. Soutoglou (Institut de Génétique et de Biologie Moléculaire et Cellulaire, Strasbourg, France), T. Misteli (National Cancer Institute, Bethesda, USA), G. Legube (Centre de Biologie Intégrative, Toulouse, France), M. Kastan (Duke Cancer Institute, Durham, USA), A. Aguilera, (Centro Andaluz de Biología Molecular y Medicina Regenerativa, Sevilla, Spain), Y. Xu (University of California, San Diego, USA), S. P. Jackson (Gurdon Institute, Cambridge, UK), D. Durocher (The Lunenfeld-Tanenbaum Research Institute, Toronto, Canada), B. Amati (European Institute of Oncology, Milan, Italy), A. Verrecchia (European Institute of Oncology, Milan, Italy), P. Pellanda (European Institute of Oncology, Milan, Italy) for reagents; Single Molecule Analysis in Real-Time Center (University of Michigan, USA) for instruments; M. Bedford (MD Anderson Cancer Center, Texas, USA), C. A. Sagum (MD Anderson Cancer Center, Texas, USA) and M. Roncador (Italian National Research Council, Pavia, Italy) for their help during the revision of the manuscript and all F.d'A.d.F. group members for reading the manuscript, support and constant discussions. F.M. was supported by Fondazione Italiana Ricerca Sul Cancro (FIRC, 12491). S.F. was supported by Collegio Ghislieri and Fondazione Cariplo (Grant rif. 2014-1215). G.V.S. is supported by Mechanobiology Institute (MBI) and Singapore Ministry of Education Academic Research Fund Tier3 (MOE2012-T3-1-001). N.G.W. is supported by NIH grants 2R01 GM062357, 1R01 GM098023 and 1R21 AI109791. F.d'A.d.F. was supported by the Associazione Italiana per la Ricerca sul Cancro, AIRC (application 12971), Human Frontier Science Program (contract RGP 0014/2012), Cariplo Foundation (grant 2010.0818 and 2014-0812), Marie Curie Initial Training Networks (FP7 PEOPLE 2012 ITN (CodAge)), Fondazione Telethon (GGP12059), Association for International Cancer Research (AICR-Worldwide Cancer Research Rif. N. 14-1331), Progetti di Ricerca di Interesse Nazionale (PRIN) 2010–2011, the Italian Ministry of Education Universities and Research EPIGEN Project, a European Research Council advanced grant (322726) and AriSLA (project 'DDRNA and ALS').

AUTHOR CONTRIBUTIONS

S.P. conceived and performed all microinjection assays, intracellular single-molecule imaging of DDRNA, FISH and kinetics experiments. V.V. generated the lentiviral I-SceI-GR construct, produced strand-specific RT–qPCR data for dilncRNA detection (NIH2/4 cells, NIH3T3duo cells, U2OS19ptight cells, HeLa111 cells, HeLa I-PpoI cells cut in the DAB1 gene) and qPCR analyses of ChIP experiments in NIH2/4 and determined dilncRNA polyadenylation status. S.S. performed all *in vitro* DSB-induced transcription assays and 5′ RACE and produced samples for sequencing. U.G. performed the RNA pulldown experiments without ASOs and RIP experiments, performed RT–qPCR analyses of DDRNA and generated the GFP-53BP1ΔTUD construct. M.C. performed ChIP experiments of RNAPII and the phosphorylated forms in NIH2/4 cells and the ChIP in AsiSI-ER BJ-5Ta cells treated with DRB. F.P. performed the *in vitro* binding assay of RNAPII to DNA ends, the co-immunoprecipitations of RNAPII with MRN and the ChIP of RNAPII in HeLa I-PpoI cells. Y.W. performed confocal and super-resolution analyses of RNAPII localization on damaged chromatin. F.I. conducted bioinformatics analyses of next-generation sequencing data. I.C. detected dilncRNA in the AsiSI

© 2017 Macmillan Publishers Limited, part of Springer Nature. All rights reserved.

system. V.M. contributed with technical support. S.F. supervised M.C. and I.C. G.V.S. supervised Y.W. N.G.W. initiated the single-molecule experiments, advised S.P. in their execution, provided critical input in experimental design and result interpretation, and edited the manuscript. F.M. designed and performed all of the remaining experiments and wrote the manuscript. F.d'A.d.F. conceived the study and, together with F.M., assembled and revised the manuscript. All authors commented on the manuscript.

COMPETING FINANCIAL INTERESTS

F.d'A.d.F., F.M. and S.F. are inventors on the following patent application: PCT/EP2013/059753.

Published online at http://dx.doi.org/10.1038/ncb3643
Reprints and permissions information is available online at www.nature.com/reprints
Publisher's note: Springer Nature remains neutral with regard to jurisdictional claims in published maps and institutional affiliations.

1. Polo, S. E. & Jackson, S. P. Dynamics of DNA damage response proteins at DNA breaks: a focus on protein modifications. *Genes Dev.* **25,** 409–433 (2011).
2. Sharma, V. & Misteli, T. Non-coding RNAs in DNA damage and repair. *FEBS Lett.* **587,** 1832–1839 (2013).
3. Derr, L. K. & Strathern, J. N. A role for reverse transcripts in gene conversion. *Nature* **361,** 170–173 (1993).
4. Storici, F., Bebenek, K., Kunkel, T. A., Gordenin, D. A. & Resnick, M. A. RNA-templated DNA repair. *Nature* **447,** 338–341 (2007).
5. Keskin, H. *et al.* Transcript-RNA-templated DNA recombination and repair. *Nature* **515,** 436–439 (2014).
6. Wei, W. *et al.* A role for small RNAs in DNA double-strand break repair. *Cell* **149,** 101–112 (2012).
7. Wang, Q. & Goldstein, M. Small RNAs recruit chromatin-modifying enzymes MMSET and Tip60 to reconfigure damaged DNA upon double-strand break and facilitate repair. *Cancer Res.* **76,** 1904–1915 (2016).
8. Gao, M. *et al.* Ago2 facilitates Rad51 recruitment and DNA double-strand break repair by homologous recombination. *Cell Res.* **24,** 532–541 (2014).
9. Qi, Y., Zhang, Y., Baller, J. A. & Voytas, D. F. Histone H2AX and the small RNA pathway modulate both non-homologous end-joining and homologous recombination in plants. *Mutat. Res.* **783,** 9–14 (2016).
10. Yang, Y. G. & Qi, Y. RNA-directed repair of DNA double-strand breaks. *DNA Repair* **32,** 82–85 (2015).
11. Ohle, C. *et al.* Transient RNA-DNA hybrids are required for efficient double-strand break repair. *Cell* **167,** 1001–1013 e1007 (2016).
12. Chakraborty, A. *et al.* Classical non-homologous end-joining pathway utilizes nascent RNA for error-free double-strand break repair of transcribed genes. *Nat. Commun.* **7,** 13049 (2016).
13. Mochizuki, K., Fine, N. A., Fujisawa, T. & Gorovsky, M. A. Analysis of a piwi-related gene implicates small RNAs in genome rearrangement in tetrahymena. *Cell* **110,** 689–699 (2002).
14. Schmidts, I., Bottcher, R., Mirkovic-Hosle, M. & Forstemann, K. Homology directed repair is unaffected by the absence of siRNAs in *Drosophila melanogaster*. *Nucleic Acids Res.* **44,** 8261–8271 (2016).
15. Miki, D. *et al.* Efficient generation of diRNAs requires components in the posttranscriptional gene silencing pathway. *Sci. Rep.* **7,** 301 (2017).
16. Francia, S. *et al.* Site-specific DICER and DROSHA RNA products control the DNA-damage response. *Nature* **488,** 231–235 (2012).
17. Francia, S., Cabrini, M., Matti, V., Oldani, A. & d'Adda di Fagagna, F. DICER, DROSHA and DNA damage response RNAs are necessary for the secondary recruitment of DNA damage response factors. *J. Cell Sci.* **129,** 1468–1476 (2016).
18. Rossiello, F. *et al.* DNA damage response inhibition at dysfunctional telomeres by modulation of telomeric DNA damage response RNAs. *Nat. Commun.* **8,** 13980 (2017).
19. Michalik, K. M., Bottcher, R. & Forstemann, K. A small RNA response at DNA ends in *Drosophila*. *Nucleic Acids Res.* **40,** 9596–9603 (2012).
20. Soutoglou, E. *et al.* Positional stability of single double-strand breaks in mammalian cells. *Nat. Cell Biol.* **9,** 675–682 (2007).
21. Pitchiaya, S., Androsavich, J. R. & Walter, N. G. Intracellular single molecule microscopy reveals two kinetically distinct pathways for microRNA assembly. *EMBO Rep.* **13,** 709–715 (2012).
22. Pitchiaya, S., Krishnan, V., Custer, T. C. & Walter, N. G. Dissecting non-coding RNA mechanisms in cellulo by single-molecule high-resolution localization and counting. *Methods* **63,** 188–199 (2013).
23. Pitchiaya, S., Heinicke, L. A., Park, J. I., Cameron, E. L. & Walter, N. G. Resolving subcellular miRNA trafficking and turnover at single-molecule resolution. *Cell Rep.* **19,** 630–642 (2017).
24. Bensaude, O. Inhibiting eukaryotic transcription: which compound to choose? How to evaluate its activity? *Transcription* **2,** 103–108 (2011).
25. Raj, A., van den Bogaard, P., Rifkin, S. A., van Oudenaarden, A. & Tyagi, S. Imaging individual mRNA molecules using multiple singly labeled probes. *Nat. Methods* **5,** 877–879 (2008).
26. Lemaitre, C. *et al.* The nucleoporin 153, a novel factor in double-strand break repair and DNA damage response. *Oncogene* **31,** 4803–4809 (2012).
27. Lemaitre, C. *et al.* Nuclear position dictates DNA repair pathway choice. *Genes Dev.* **28,** 2450–2463 (2014).
28. Roukos, V. *et al.* Spatial dynamics of chromosome translocations in living cells. *Science* **341,** 660–664 (2013).
29. Pankotai, T., Bonhomme, C., Chen, D. & Soutoglou, E. DNAPKcs-dependent arrest of RNA polymerase II transcription in the presence of DNA breaks. *Nat. Struct. Mol. Biol.* **19,** 276–282 (2012).
30. Iacovoni, J. S. *et al.* High-resolution profiling of γH2AX around DNA double strand breaks in the mammalian genome. *EMBO J.* **29,** 1446–1457 (2010).
31. Asada, K. *et al.* Rescuing dicer defects via inhibition of an anti-dicing nuclease. *Cell Rep.* **9,** 1471–1481 (2014).
32. Feuerhahn, S., Iglesias, N., Panza, A., Porro, A. & Lingner, J. TERRA biogenesis, turnover and implications for function. *FEBS Lett.* **584,** 3812–3818 (2010).
33. Wang, Y., Maharana, S., Wang, M. D. & Shivashankar, G. V. Super-resolution microscopy reveals decondensed chromatin structure at transcription sites. *Sci. Rep.* **4,** 4477 (2014).
34. Dupre, A. *et al.* A forward chemical genetic screen reveals an inhibitor of the Mre11–Rad50–Nbs1 complex. *Nat. Chem. Biol.* **4,** 119–125 (2008).
35. Kumar, R. & Cheok, C. F. RIF1: a novel regulatory factor for DNA replication and DNA damage response signaling. *DNA Repair (Amst)* **15,** 54–59 (2014).
36. Goodarzi, A. A. & Jeggo, P. A. The heterochromatic barrier to DNA double strand break repair: how to get the entry visa. *Int. J. Mol. Sci.* **13,** 11844–11860 (2012).
37. Smeenk, G. & Mailand, N. Writers, readers, and erasers of histone ubiquitylation in DNA double-strand break repair. *Front. Genet.* **7,** 122 (2016).
38. Pryde, F. *et al.* 53BP1 exchanges slowly at the sites of DNA damage and appears to require RNA for its association with chromatin. *J. Cell Sci.* **118,** 2043–2055 (2005).
39. Fradet-Turcotte, A. *et al.* 53BP1 is a reader of the DNA-damage-induced H2A Lys 15 ubiquitin mark. *Nature* **499,** 50–54 (2013).
40. Burger, K. *et al.* Nuclear phosphorylated Dicer processes double-stranded RNA in response to DNA damage. *J. Cell Biol.* **216,** 2373–2389 (2017).
41. Holoch, D. & Moazed, D. RNA-mediated epigenetic regulation of gene expression. *Nat. Rev. Genet.* **16,** 71–84 (2015).
42. Guil, S. & Esteller, M. RNA-RNA interactions in gene regulation: the coding and noncoding players. *Trends Biochem. Sci.* **40,** 248–256 (2015).
43. Vitelli, V. *et al.* Recent advancements in DNA damage-transcription crosstalk and high-resolution mapping of DNA breaks. *Annu. Rev. Genomics Hum. Genet.* **18,** 87–113 (2017).
44. Proudfoot, N. J. Transcriptional termination in mammals: stopping the RNA polymerase II juggernaut. *Science* **352,** aad9926 (2016).
45. Skourti-Stathaki, K., Kamieniarz-Gdula, K. & Proudfoot, N. J. R-loops induce repressive chromatin marks over mammalian gene terminators. *Nature* **516,** 436–439 (2014).
46. Capozzo, I., Iannelli, F., Francia, S. & d'Adda di Fagagna, F. Express or repress? The transcriptional dilemma of damaged chromatin. *FEBS J.* **284,** 2133–2147 (2017).
47. Iannelli, F. *et al.* A damaged genome's transcriptional landscape through multilayered expression profiling around *in situ*-mapped DNA double-strand breaks. *Nat. Commun.* **8,** 15656 (2017).
48. Britton, S. *et al.* DNA damage triggers SAF-A and RNA biogenesis factors exclusion from chromatin coupled to R-loops removal. *Nucleic Acids Res.* **42,** 9047–9062 (2014).
49. Boeing, S. *et al.* Multiomic analysis of the UV-induced DNA damage response. *Cell Rep.* **15,** 1597–1610 (2016).
50. Kakarougkas, A. *et al.* Requirement for PBAF in transcriptional repression and repair at DNA breaks in actively transcribed regions of chromatin. *Mol. Cell* **55,** 723–732 (2014).

© 2017 Macmillan Publishers Limited, part of Springer Nature. All rights reserved.

DOI: 10.1038/ncb3643

METHODS

Cell culture, transfection and ionizing radiation. NIH2/4 cells (gift from E. Soutoglou), a NIH3T3-derived cell line bearing the Lac-I-SceI-Tet construct[20], were grown in DMEM (Lonza), supplemented with 10% fetal bovine serum (FBS) tetracycline-tested, 1% L-glutamine and hygromycin (400 μg ml^{-1}). NIH3T3duo cells (gift from T. Misteli), a NIH3T3-derived cell line bearing one LacO-I-SceI and three TetO-I-SceI-TetO plasmids[28], were grown in DMEM (Lonza), supplemented with 10% FBS tetracycline-tested, 1% L-glutamine, IPTG (5 mM) and doxycycline (1 μg ml^{-1}). To induce LacR and TetR binding, cells were washed extensively in PBS and grown in medium without IPTG and doxycycline.

Where indicated, Cherry-LacR- or YFP-TetR- (1 μg per well) and constitutive I-SceI- (2 μg per well) expressing vectors (gift from E. Soutoglou) were transfected in NIH2/4 cells by Lipofectamine 2000 according to the manufacturer's protocol (Life Technologies). To induce YFP-TetR binding to the TetO array, doxycycline (1 μg ml^{-1}) was added to the culture medium for at least 3 h. GFP-LacR plasmid was created by ligating the LacR insert into the BspEI-BamHI sites of a pEGFP-C1 (Clontech) plasmid. The LacR insert was originally obtained from the Cherry-LacR plasmid via a BspEI-BamHI double digestion.

For microinjection experiments, 1 × 10^5 cells were seeded onto delta T dishes (Bioptechs) one day before microinjection, so that they were ∼80% confluent at the time of microinjection. Regular medium was replaced with a minimal medium (HBS) without serum, but containing 20 mM HEPES-KOH pH 7.4, 135 mM NaCl, 5 mM KCl, 1 mM $MgCl_2$, 1.8 mM $CaCl_2$ and 5.6 mM glucose, immediately before microinjection. After microinjection, cells were incubated in phenol red-free DMEM containing 10% (v/v) FBS in the presence of 5% CO_2 at 37 °C for the indicated amounts of time prior to imaging. For plasmid co-transfections, 250–1,000 ng of GFP-LacR and/or Cherry-53BP1 (19835, Addgene) and 750 ng of pLacZ (uncut), constitutive I-SceI expression vector (cut) or inducible I-SceI-GR-RFP (17654, Addgene) expression vector (cut) were mixed with 2.5 μl of Lipofectamine2000 per Delta T dish. Plasmids and Lipofectamine were diluted in 100 μl of OptiMEM (GIBCO) each and added to 1 ml of medium in the dish. Cells were used for experiments 24 h post transfection.

Where indicated, 1 μg of mammalian RNaseH1 expressing plasmid (gift from A. Aguilera) or an empty vector control was co-transfected with YFP-TetR- and I-SceI-expressing vectors in NIH2/4 cells.

U2OS19ptight[26] (gift from E. Soutoglou) were grown in DMEM without phenol red (GIBCO), supplemented with 10% FBS tetracycline-tested, 1% L-glutamine and G418 (800 μg ml^{-1}). To induce I-SceI expression, cells were incubated with doxycycline (1 μg ml^{-1}) for 16 h.

AsiSI-ER-U20S cells[30] (gift from G. Legube) were cultured in Dulbecco's modified Eagle's medium (DMEM) without phenol red supplemented with glutamine, pyruvate, HEPES and 10% FBS (Euroclone). Cells were selected with puromycin at a final concentration of 1 μg ml^{-1}. For AsiSI-dependent DSB induction, cells were treated with 300 nM 4-OHT (Sigma-Aldrich) for 4 h.

BJ hTERT Hygro (ATCC, BJ-5Ta) HA-AsiSI-ER were grown in DMEM without phenol red supplemented with 10% fetal bovine serum (FBS), 1% L-glutamine, 20% M199, hygromycin (10 μg ml^{-1}) and puromycin (1 μg ml^{-1}). To generate the AsiSI-ER BJ-5Ta cell line, pBABE HA-AsiSI-ER plasmid (gift from G. Legube) was retroviral infected using a standard calcium phosphate transfection/infection protocol (1:8 virus dilution used). The selection was performed using 2 μg ml^{-1} puromycin. For AsiSI-ER induction, cells were treated with 300 nM 4-OHT (Sigma-Aldrich) overnight.

HeLa cells (ATCC) and HeLa111 cells (gift from E. Soutoglou), a HeLa-derived cell line bearing one LacO-I-SceI plasmid[27], were grown under standard tissue culture conditions (37 °C, 5% CO2) in MEM+Glutamax (GIBCO), supplemented with 10% FBS, 1% non-essential amino acids and 1% sodium pyruvate. Where indicated, 1 μg of mammalian ER-I-PpoI-expressing plasmid (gift from M. Kastan) or an empty vector control was transfected in HeLa cells, grown in their medium without phenol red. Twenty-four hours later, to activate the nuclear translocation of ER-I-PpoI, cells were treated with 4-OHT (Sigma-Aldrich) at 2 μM final concentration for 3 h. Where indicated, 1 μg of CRISPR–Cas9-expressing plasmid (gift from B. Amati) or an empty vector control was transfected in NIH2/4 cells. RNA was collected 24 h later. See Supplementary Table 2 for the sequence of the guide RNA.

Human normal foreskin fibroblasts (BJ, ATCC) were grown in MEM+Glutamax (GIBCO), supplemented with 10% FBS, 1% non-essential amino acids and 1% sodium pyruvate.

Mouse embryonic stem cells (mESCs) *Atm*$^{+/+}$ and *Atm*$^{-/-}$ (gift from Y. Xu) were grown in stem cell medium (DMEM Glutamax, 1% non-essential amino acids, 1% sodium pyruvate, 0.2% 2-mercaptoethanol, 15% FCS and 0.2% LIF) on gelatin-coated plates.

All cell lines are tested for mycoplasma at each batch freezing by PCR and by a biochemical test (MycoAlert, Lonza).

Ionizing radiation (IR, 2 Gy unless specified otherwise) was induced by a high-voltage X-ray generator tube (Faxitron X-Ray Corporation). For the analysis of DDR markers, cells were fixed at 10 min or 1 h post IR.

Antibodies. Primary antibodies for immunofluorescence: γH2AX pS139 (mouse, Millipore 05-636, 1:1,000), ATM pS1981 (mouse, Rockland 200-301-400, 1:400), 53BP1 (rabbit, Novus Biologicals NB100-304, 1:1,000), RNAPII pSer5 (rabbit, Abcam ab5131, 1:500), RNaseH1 (rabbit, Proteintech 15606-1-AP, 1:200), RIF1 (rabbit, Bethyl A300-569A, 1:1,000), pKAP1 (rabbit, Bethyl A300-767A, 1:1,000), RNF168 (rabbit, Millipore Abe367, 1:500), mono- and polyubiquitylated conjugates monoclonal antibody (FK2, Enzo Life Sciences BML-PW8810-0100, 1:1,000). Secondary antibodies for immunofluorescence: donkey anti-mouse or anti-rabbit Alexa 405 (1:200), Alexa 488 (1:500) or Alexa 647 (1:500) IgG (Life Technologies) or goat anti-mouse or anti-rabbit Cy5 (Jackson Immunoresearch). The following antibodies were used for ChIP: RNAPII N-20 (rabbit, Santa Cruz, sc899x, 2 μg) for mouse cells; total RNAPII (mouse, Abcam, ab817, 5 μg); RNAPII pSer2 (rabbit, Abcam ab5095, 2 μg) for human cells; RNAPII pSer5 (rabbit, Abcam ab5131, 2 μg); γH2AX pS139 (rabbit, Abcam ab2893, 2 μg); 53BP1 (rabbit, Novus Biologicals NB100-305, 3 μg). Primary antibodies for immunoprecipitation and western blot: RNAPII (POLR2A) (mouse, Santa Cruz 8WG16, IP: 5 μg per 1 mg of total proteins, WB: 1:50); MRE11 (rabbit polyclonal raised against recombinant human MRE11, gift from S. P. Jackson; validation data using MRE11-deficient cells or purified recombinant MRN are available upon request; IP: 1 μg per 1 mg of total proteins, WB: 1:1,000); NBS1 (rabbit, Novus Biologicals NB100-143 IP: 1 μg per 1 mg of total proteins, WB: 1:1,000); RAD50 (Millipore (13B3/2C6) 05-525 IP: 1 μg per 1 mg of total proteins, WB: 1:1,000); RNAPII pSer2 (rabbit, Abcam ab5095 WB: 1:1,000); RNAPII pSer5 (rabbit, Abcam ab5131 WB: 1:1,000).

Lentiviral infection. Lentiviral empty vector was obtained by removing the I-SceI-BFP cassette between XhoI and XbaI sites from the lentiviral backbone pCVL-HA-NLS-I-SceI-BFP (45574, Addgene). Lentiviral I-SceI-GR (which is the inducible I-SceI in the main text) was obtained by PCR amplification of the I-SceI-GR cassette (17654, Addgene) with adapter primers containing XhoI–XbaI sites and subsequent cloning into the lentiviral empty vector. Where indicated, target cells (NIH2/4, NIH3T3duo and HeLa111 cells for dilncRNA induction experiments) were incubated with viral supernatant diluted 1:4 in medium supplemented with 8 μg ml^{-1} Polybrene for 16 h. Three days post infection, I-SceI-GR translocation to the nucleus was induced by adding triamcinolone acetonide 0.1 μM (TA, Sigma-Aldrich) to the medium for 1 h.

RNA extraction. Total RNA was isolated from cells using either RNAeasy kit (Qiagen) or Maxwell RSC simplyRNA Tissue Kit (Promega), according to the manufacturer's instructions. Where specified, chromatin-bound RNA was extracted as follows. Cells were fractionated following a published protocol[51]. After recovery of the chromatin fraction, 50 U of Turbo DNase (Ambion) was added to the pellet and incubated at 37 °C for 10 min, following by digestion with 200 μg of Proteinase K (Roche) at 37 °C for 10 min. The RNA was then purified with phenol–chloroform and isolated as the total RNA.

For gel-extraction experiments, total RNA was purified using the Maxwell miRNA Tissue Kit with the Maxwell RSC Instrument (Promega) and loaded onto 10% Urea-PAGE. For gel-extracted small RNA analysis, a *Caenorhabditis elegans* miRNA was used as spike-in before loading.

Standard RT–qPCR and strand-specific RT–qPCR. For standard RT–qPCR, cDNA was generated using the SuperScript VILO Reverse Transcriptase (Life Technologies). Roche SYBR Green-based RT–qPCR experiments were performed on a Roche LightCycler 480.

For DSB-induced transcripts detection, total RNA was extracted using RNeasy RNA extraction kit (Qiagen). Samples were treated with DNaseI (Qiagen) to remove any potential residual genomic DNA contamination. Five hundred nanograms of total RNA was reverse-transcribed using the Superscript First Strand cDNA synthesis kit (Invitrogen) with strand-specific primers. Expression of DSB-induced transcripts was determined by RT–qPCR using Roche SYBR green, EvaGreen Supermix (Bio-Rad) or QuantiTect SYBR (Qiagen) reagents. For each RT–qPCR reaction, 25 ng of cDNA was used. To amplify Lac and Tet repeats, we adapted a technique, as previously described[52].

For DDRNA and pre-DDRNA detection, gel-extracted RNA fractions were retro-transcribed using the miScript II RT Kit (Qiagen), according to the manufacturer's instructions. For gel-extracted DDRNA analysis, the spike-in was used as a normalizer. For gel-extracted pre-DDRNA analysis, 5S ribosomal RNA was used as a normalizer.

See Supplementary Table 1 for a complete list of primers used.

© 2017 Macmillan Publishers Limited, part of Springer Nature. All rights reserved.

Single-molecule fluorescence *in situ* hybridization (smFISH). NIH2/4 cells were transfected with LacR-GFP- and I-SceI-GR-RFP-expressing plasmids and incubated for 24 h. Nuclear translocation of I-SceI-GR-RFP was induced by treating cells with 0.1 μM TA (cut) or ethanol (uncut) for 1 h. When mentioned, cells were treated with DRB (100 μM) or DMSO for 2 h prior to induction and during induction. When mentioned, cells were treated with mirin (100 μM) or DMSO for 30 min prior to induction and during induction. When mentioned, cells were RNaseA-treated (1 μg μl^{-1}) in DPBS at 37 °C, prior to probe treatment. smFISH was performed as described previously[18]. When mentioned, cells were RNaseH treated (1 μg μl^{-1}) in DPBS at 37 °C, prior to mounting. Images were analysed using custom-written macros in ImageJ and Imaris.

See Supplementary Table 1 for FISH probe sequences.

Inhibition of RNA transcription. Actinomycin D (ACTD) at low dose (0.05 μg ml^{-1}) is a specific inhibitor of RNAPI; ACTD at high dose (2 μg ml^{-1}) and α-amanitin (50 μg ml^{-1}) are specific inhibitors of RNAPII; 5,6-dichloro-1-β-D-ribofuranosylbenzimidazole (DRB, 100 μM) is a specific inhibitor of RNAPII elongation. ACTD and DRB were dissolved in DMSO; α-amanitin was dissolved in deionized water. For α-amanitin treatments, cells were mildly permeabilized by 0.6% (NIH2/4 cells) or 2% (HeLa and BJ cells) Tween20 in PBS for 10 min at room temperature. Permeabilized cells were then incubated in OptiMEM medium with α-amanitin at 37 °C for the indicated time before DNA damage induction. Specificity and efficacy of the drugs were monitored by analysing by RT–qPCR the levels of known short-lived RNAs that are specifically transcribed by one of the different RNA polymerases: 47S RNA (ribosomal RNA precursor) for RNAPI; c-fos RNA for RNAPII; 7SK RNA for RNAPIII. Unless specified otherwise, cells were pre-treated with RNAPII inhibitors for 2 h before DNA damage and analysed 1 h later. For DNA repair experiments, BJ cells were pre-treated with DRB 100 μM for 2 h, irradiated (2 Gy) and analysed at 1 h and 5 h post irradiation.

Nuclei isolation, immunostaining, confocal imaging and image analysis. NIH2/4 cells were transfected with a constitutively active I-SceI or an empty vector. Cells were fixed and treated with 4% Triton-X in TM2 buffer[33] with 1× protease inhibitor cocktail to remove cytoplasm. Isolated nuclei were incubated in 5% BSA, followed by incubation with primary and secondary antibodies. Nuclei were labelled with YOYO-1 followed by hypotonic treatment. Samples were imaged on a Nikon A1R using 100×, 1.4 NA oil objective, 3× magnification, and a *z*-step of 500 nM. The enrichment index was defined as the ratio between the mean intensity of γH2AX or RNAPII pSer5 at the LacR spot and the mean intensity of γH2AX or RNAPII pSer5 throughout the three-dimensional nuclear region.

Chromatin spread preparation, immunostaining, super-resolution imaging and imaging analysis. After NIH2/4 cells were fixed and quenched, cells were treated with trypsin (GIBCO) and resuspended with culture medium. Chromatin spreads were prepared according to the methods previously described[33]. Super-resolution imaging was performed on a Zeiss Elyra P.1 microscope equipped with an oil-immersion objective, and images were analysed according to the procedures previously described[33].

Chromatin immunoprecipitation (ChIP). NIH2/4 cells expressing the inducible I-SceI were induced or mock induced for 1 h before crosslinking. For the experiment with the MRN inhibitor, NIH2/4 cells expressing the inducible I-SceI were treated with mirin (100 μM) or DMSO for 2 h prior the induction and during I-SceI induction. AsiSI-ER BJ-5Ta cells were treated with 300 nM 4-OHT overnight and treated with DRB or DMSO for 3 h before crosslinking. HeLa cells were transfected with I-PpoI-ER and ASOs (see the 'Antisense oligonucleotides' section) and 24 h later treated with 2 μM 4-OHT for 3 h before crosslinking. ChIP was performed as described previously[47]. ChIP in HeLa cells cut by I-PpoI was performed as described previously[53]. Briefly, cells were crosslinked in 1% PFA and sonicated with a Bioruptor sonicator to obtain 250 bp resolution. One hundred micrograms of chromatin was used per sample.

Immunoprecipitation. HEK293 cells irradiated (4 Gy) or not irradiated were collected 10 min post IR and washed in 1×TBS (ice cold) and resuspended in 0.5 ml of lysis buffer (50 mM Tris, pH 7.5; 150 mM NaCl; 0.5% NP-40; 5 mM $MgCl_2$; 5% glycerol; 1× Protease inhibitors (Roche tablet); 1× phosphatase inhibitors tablet (Roche)) supplemented with 1 μl per 1 ml Benzonase (250 units ml^{-1}, Sigma). Lysates were incubated at 4 °C for 45 min. Lysates were cleared and equal amounts of total protein extracts were used for each sample and primary antibody, pre-incubated with G Dynabeads (Invitrogen), was added and left at 4 °C on a wheel for a further 2 h. The beads were gently collected using a magnet rack (Invitrogen) and washed six times with 1× lysis buffer and resuspended in 50 μl of sample loading buffer (Invitrogen).

***In vitro* RNAPII binding to DNA ends.** HeLA nuclear extracts were prepared according to a modified Dignam protocol[54].

Biotinylated primers were used to PCR amplify the DNA fragment containing I-SceI and Lac and Tet repeats from the pLac-Tet plasmid containing an I-SceI site flanked by three Tet and eight Lac elements into the pMK-RQ vector (GENEART). The PCR fragment was then purified by ReverseQ column binding and eluted by a salt gradient. One microgram of the correct fragment was incubated in I-SceI NEB buffer with 5 μl of streptavidin magnetic beads (Invitrogen) at room temperature for 30 min, and subsequently at 37 °C for 1 h in the presence of 1 μl I-SceI enzyme (NEB). Magnetic beads were then washed three times in cold 1× TBS and then incubated at 16 °C with HeLa cell nuclear extract for 1 h. After three washes in cold TBS, beads were boiled in 2× Invitrogen sample buffer and samples were analysed by western blot. As a control for cutting efficiency, 1/10 of beads was collected and incubated with proteinase K; DNA was then recovered by phenol/chloroform/isoamyl alcohol extraction and loaded on an agarose gel. See Supplementary Table 1 for the complete list of primers used.

***In vitro* transcription assay.** *In vitro* transcription was performed using cell-free extracts from the K562 cell line[54]. Two micrograms cell-free extracts was incubated with 200 ng of linearized plasmid prepared by digesting the pLac-Tet plasmid (GENEART) with I-SceI, in a buffer containing 20 mM HEPES (pH 7.5), 3 mM $MgCl_2$, 100 mM KCl, 0.2 mM EDTA, 0.5 mM dithiothreitol (DTT), 20% glycerol, 0.4 mM rATP, rCTP, rGTP each and 10 μCi [α-^{32}P]UTP for 1 h at 37 °C in a total reaction volume of 25 μl. The reaction was stopped by the addition of 0.3 M Tris-HCl (pH 7.4 at 25 °C), 0.3 M sodium acetate, 0.5% SDS, 2 mM EDTA and 3 μg ml^{-1} glycogen, purified by phenol–chloroform extraction and precipitated. Dried pellets were resuspended in RNase-free water and, when mentioned, incubated with increasing concentrations of RNaseA or DNaseI at 37 °C for 30 min. Samples were then mixed with an equal volume of gel loading buffer containing 98% formamide, 10 mM EDTA, 0.1% xylene cyanol, 0.1% bromophenol blue, heated at 80 °C and loaded onto an 8% denaturing PAGE. The gel was dried, exposed to a phosphorimaging screen and acquired using a Typhoon phosphorimaging system (GE Healthcare).

Plasmids (pBluescript or pUC19) were digested with BamHI, EcoRI, EcoRV, SmaI, KpnI and SacI to generate ends containing 5′-GATC, 5′-AATT, blunt GAT, blunt CCC, GTAC-3′ and AGCT-3′, respectively, and purified. Transcription was performed as mentioned above.

For the experiments with RNAPII, ATM and PI(3)K-like kinase inhibitors, 2 μg of cell extracts was incubated with increasing concentrations of the inhibitors in the transcription reaction, incubated on ice for 15 min, shifted to 37 °C for 30 min, followed by addition of the linearized pLac-Tet plasmid substrate and incubation for 1 h at 37 °C. Reaction products were resolved as explained earlier. Cell-free extracts prepared from mESCs ATM$^{+/+}$ and ATM$^{-/-}$ were prepared as described earlier.

RNA-seq. RNA generated from *in vitro* transcription with circular and linearized pLac-Tet plasmid was treated with DNaseI and size-selected by gel purification to exclude RNA shorter than 50 bp. After fluorometric quantification by Qubit (Life Technologies), RNA was used for library preparation with Ion Total RNA-Seq Kit v2 for strand-specific RNA sequencing. The obtained libraries were pooled and sequenced on the Ion PI chip (Life Technologies). Reads were mapped to the pLac-Tet plasmid using Bowtie2 (ref. 55) with a very sensitive local option. The coverage of each position was calculated using samtools mpileup[56].

Rapid amplification of cDNA ends (RACE). 5′ RACE was performed using the FirstChoice 5′ RLM-RACE kit (Life Technologies). Briefly, *in vitro* reaction products from linearized pLac-Tet plasmid with or without extracts were treated with calf intestinal phosphatase (CIP) and tobacco acid pyrophosphatase (TAP), followed by ligation with an adapter, following the manufacturer's protocol. The products were reverse-transcribed, PCR-amplified using primers (Supplementary Table 1) matching the sequences outside the Lac and Tet repeats, cloned into TA vector (Invitrogen) and sequenced by the Sanger method.

RNA oligonucleotides. RNA oligonucleotides were synthesized with a 5′ phosphate and HPLC purified (Integrated DNA Technologies). For fluorophore-labelled oligonucleotides, Alexa 647-NHS and Cy5-NHS were conjugated to the 3′ end. Annealing of complementary sequences was performed in a 1:1 ratio in 1× PBS or 1× siRNA buffer (GE Healthcare, Dharmacon). See Supplementary Table 2 for the complete list of RNA oligonucleotides used.

Microinjection. Injections were performed as described previously[23]. For DDRNA microinjections, the micropipette (Femtotips, Eppendorf) was loaded with 0.125–2 μM Alexa647-labelled DDRNAs and 0.025–0.05% (w/v) 10 kDa cascade blue dextran (Invitrogen) in 1× PBS. For BSA (NEB) or I-SceI (NEB) co-injections,

© 2017 Macmillan Publishers Limited, part of Springer Nature. All rights reserved.

DOI: 10.1038/ncb3643

1 μM of the appropriate protein was also added to the solution. The injection solution with these proteins also contained 3 mM Tris-HCl pH 7.4, 90 mM NaCl, 0.3 mM DTT, 0.03 mM EDTA and 15% glycerol. To inhibit transcription, 50 μg ml^{-1} α-amanitin was co-microinjected with the dsRNAs and proteins. pGFP-LacR, pCherry-53BP1 (50 ng μl^{-1}) and 100 ng μl^{-1} of pLacZ, pI-SceI were used in the plasmid injection solutions. Plasmids were diluted in solutions containing 0.025–0.05% (w/v) 10 kDa cascade blue dextran (Invitrogen) in 1× PBS. For time-lapse imaging analysis of 53BP1 focus, NIH2/4 cells expressing GFP-LacR and Cherry-53BP1 were microinjected with BSA (1 μM), I-SceI (1 μM) or I-SceI (1 μM) +α-amanitin (100 μg ml^{-1}) over a span of 5 min (referred to as the 0 min time point) and immediately imaged over a time course spanning 1 h at 0 min, 5 min, 15 min, 30 min and 60 min post injection. Image analysis was done using custom-written macros in ImageJ. The relative intensity was calculated by dividing the integrated intensity of a 50 × 50 pixel area across the 53BP1 foci (co-localizing with a GFP- LacR focus) by the intensity of a 2-pixel rim around the 50 × 50 pixel area.

Single-molecule microscopy. Single-molecule microscopy by HILO illumination was performed as described previously[23]. For multicolour live-cell imaging, the emitted light was split onto two different EMCCDs using a single beamsplitter within a filter adapter (TuCam, Andor). Emission filters were placed just prior to each camera to minimize fluorescence bleed-through. For simultaneous detection of GFP and Cy5, a filter set with a 585dxcru dichroic that splits fluorescence into et525/50m and et705/100m emission filters respectively was placed in the Tucam adapter. The et705/100m was replaced with an et630/75m emission filter for simultaneous GFP and RFP detection. Live-cell imaging and data analyses were performed as described previously[21]. For fixed-cell imaging, emission from individual fluorophores was detected one after another on a single EMCCD. Fixed-cell imaging and data analysis were performed as described previously[21] with minor modifications. In traces where the number of steps cannot be accurately determined, the average intensity of the first three frames of the trajectory was divided by that of a single photobleaching step (~2,000 a.u.) to deduce the number of molecules per particle.

RNA interference. The siGENOME smart pool siRNA oligonucleotides (Dharmacon) were transfected (20 nM) by Lipofectamine RNAiMax (Life Technologies) following the manufacturer's protocol. Seventy-two hours later, DNA damage was induced and samples were collected. See Supplementary Table 2 for the complete list of siRNAs used.

Permeabilization and incubation with DDRNA. NIH2/4 cells were seeded on coverslips and transfected with YFP-TetR- and I-SceI-expressing vectors. Twenty-four hours later, cells were permeabilized in 0.6% Tween20 (Euroclone) in sterile 1× PBS for 15 min at room temperature. After washing in sterile 1× PBS, cells were incubated in 70 μl of a solution containing sterile 1× PBS, 80 units of RNase inhibitor (RNaseOUT Life Technologies 40 units μl^{-1}) and annealed DDRNA-Cy5 (100 nM) or miRNA let-7a-Cy5 (100 nM) as a control for 30 min at room temperature. Cells were then fixed in PFA 4%, re-permeabilized in Triton 0.2% for 2 min and stained for DDR markers as described below.

Indirect immunofluorescence and imaging analysis. NIH2/4 and NIH3T3duo cells were fixed in 4% PFA for 10 min at room temperature. HeLa and BJ cells were fixed in methanol/acetone 1:1 for 2 min at room temperature or in 4% PFA. For RIF1, FK2 and RNF168 immunofluorescence, BJ cells were pre-extracted in 0.5% Triton for 5 min at 4 °C and then washed in 1× PBS and fixed in 4% PFA for 10 min at room temperature. Immunofluorescence for DDR markers was performed as described previously[16].

Immunofluorescence images of HeLa and BJ cells were acquired in parallel with identical acquisition parameters using a widefield Olympus Biosystems Microscope BX71 and the MetaMorph software (Soft Imaging System GmbH). Quantification of the number of nuclear foci per nucleus was performed with the automated image-analysis software CellProfiler 2.1.1. Cells with more than ten DDR foci were scored positive. For experiments with NIH2/4 and NIH3T3duo cells, image sections were obtained at the Delta Vision microscope (Applied Precision) by acquisition of 30 optical z-sections (0.25 μm) at different levels along the optical axis to allow a more accurate signal discrimination and detection of co-localization events. Each image was automatically subjected to deconvolution by the softWoRx software (Applied Precision). The z-sections were then loaded onto ImageJ software and z-projected to obtain a sum of image signals. For experiments with DDRNA-Cy5, cells were considered positive when there was an overlapping signal between DDRNA-Cy5 and YFP-TetR in the z-projection.

RNA pulldown. NIH2/4 cells transduced with I-SceI-GR were transfected with *in vitro*-annealed 3′-end biotinylated DDRNA (btn-L1:L2, btn-U1:U2; see the 'RNA oligonucleotides' section for sequence details) or btn-let-7a:let-7a* at the final concentration of 20 nM with Lipofectamine RNAiMAX. For the experiment with ASOs and biotinylated DDRNA, NIH2/4 cells transduced with I-SceI-GR were transfected with control ASO or specific ASOs at the final concentration of 20 nM by Lipofectamine RNAiMAX. The day after, cells were transfected with annealed btn-L1:L2 or btn-let-7a:let-7a* at the final concentration of 20 nM by Lipofectamine RNAiMAX. Twenty-four hours later, cells were treated with TA (0.1 nM) for 1 h to activate I-SceI and trypsinized. After two washes with cold 1× PBS, cell pellets were resuspended in cell lysis buffer (25 mM Tris-HCl pH 7.4, 150 mM KCl, 5 mM $MgCl_2$, 0.5% NP-40, 0.5 mM DTT, 40 U ml^{-1} of RNaseOUT and Protease Inhibitor Cocktail Set III (Merck Millipore)) for 30' at 4 °C. Streptavidin beads (Dynabeads MyOne Streptavidin C1, Life Technologies) were blocked in lysis buffer supplemented with 1 mg ml^{-1} tRNA and 1 mg ml^{-1} BSA (Ambion) for 2 h at 4 °C. Total cell extracts were cleared by centrifugation, added to the blocked beads and incubated 4 h at 4 °C. After five washes with lysis buffer, bound RNAs were isolated with proteinase K (Roche) prior to acid-phenol/chloroform (Life Technologies) extraction and ethanol precipitation. Input RNAs were treated in the same manner. Purified RNAs were treated with DNaseI (Thermo Scientific) and analysed by strand-specific RT–qPCR, as described above.

RNA immunoprecipitation (RIP). I-SceI-GR-expressing NIH2/4 cells were lysed in RIP buffer (150 mM KCl, 25 mM Tris-HCl pH 7.4, 5 % glycerol, 0.5 % NP-40, 10 mM $MgCl_2$, 1 mM $CaCl_2$, 0.5 mM DTT, 40 U ml^{-1} RNaseOUT and Protease Inhibitor Cocktail Set III) in the presence of 1,000 U ml^{-1} DNaseI (Roche). Total cell lysates were cleared by centrifugation and 5 mM EDTA was added. Before immunoprecipitation (IP), 10% of lysates was saved as RNA and protein INPUT. Ten micrograms of anti-53BP1 (NB100-304, Novus Biologicals), anti-GFP (ab290, Abcam) or normal rabbit IgGs (sc-2027) were coupled with Dynabeads Protein G (Life Technologies) for 2 h at 4 °C in RIP buffer prior to IP. IP was carried out by incubating cleared lysates with the antibody-coupled beads overnight at 4 °C. After five washes with RIP buffer, 10% of immunoprecipitated samples was eluted in SDS loading buffer for protein analysis. Bound and input RNAs were isolated as described above (see the 'RNA pulldown' section). DilncRNAs and mRNAs were analysed by qRT–PCR as already described, whereas DDRNAs and small RNAs were analysed using the miScript PCR system (Qiagen). See Supplementary Extended Data Table 1 for the complete list of primers used.

For 53BP1 ectopic expression, NIH2/4 cells were transfected with GFP-53BP1 (pcDNA-FRT/T0-eGFPnls-53BP1 1220-1631 WT, gift from D. Durocher, Addgene, 60814 (ref. 39)) or with GFP-53BP1ΔTUD plasmids. The GFP-53BP1ΔTUD construct was generated from GFP-53BP1 plasmid by inverse PCR. See Supplementary Table 1 for primer sequences.

RNaseA treatment. RNaseA treatment was performed as described previously[16]. Briefly, NIH2/4 cells expressing I-SceI were permeabilized 1 h post DSB induction and treated with RNaseA (1 mg ml^{-1}) or acetylated BSA (1 mg ml^{-1}) for 30 min at room temperature. After washes, RNase-treated cells were incubated with tRNA for 30 min. RNA was collected and equal volumes were used instrand-specific RT–qPCR.

Comet assay. The neutral comet assay was performed following the manufacturer's instructions (Trevigen). Briefly, HeLa cells were trypsinized, washed once with ice-cold PBS and resuspended in cold PBS at the final concentration of 10^5 cells ml^{-1}. Cell suspension was then combined with pre-warmed low-melting agarose at a ratio of 1:10 and poured onto the slides. Lysis was performed overnight at 4 °C. Electrophoresis was carried out in 1× Neutral Electrophoresis Buffer for 45 min at 21 V. After DNA precipitation and washing in 70% ethanol, slides were dried and DNA was stained with SYBR Gold (Thermo Fisher) before epifluorescence microscopy analysis (Olympus Biosystems). The comet tail moment was calculated using OpenComet software.

Antisense oligonucleotides. Locked nucleic acid ASOs (Exiqon) were co-transfected with Cherry-LacR- and I-SceI-expressing vectors in NIH2/4 cells by Lipofectamine 2000. ASOs (0.2 nM) were first boiled at 90 °C for 5 min and immediately transferred into ice for 5 min and then added in different combinations to a transfection mix containing Cherry-LacR- and I-SceI-expressing vectors. At 24 h post transfection, cells were scored for DDR markers at the LacR locus. For the DNA repair experiment, I-SceI-GR translocation to the nucleus was induced by adding TA 0.1 nM to the medium for 3 h. After extensive washes in PBS, medium was replaced and DNA repair was allowed for 24 h.

ASOs (20 nM) were co-transfected with I-SceI-expressing vector in NIH3T3duo cells by Lipofectamine 2000, as described above. At 24 h post transfection, cells were scored for DDR markers at the LacR and TetR loci. See Supplementary Table 3 for the ASO sequences used in NIH2/4 and in NIH3T3duo cells.

© 2017 Macmillan Publishers Limited, part of Springer Nature. All rights reserved.

Locked nucleic acid ASOs (Exiqon) were co-transfected with I-PpoI-expressing vectors in HeLa cells by Lipofectamine 2000. ASOs (20 nM final concentration of the pooled ASOs) were first boiled at 90 °C for 5 min and immediately transferred into ice for 5 min and then added in different combinations to a transfection mix containing I-PpoI-expressing vector. At 24 h post transfection, ER-I-PpoI was induced by 4-OHT (Sigma-Aldrich) at 2 μM final concentration for 3 h and samples were collected for ChIP experiments. See Supplementary Table 3 for DAB1-specific ASO sequences.

Statistics and reproducibility. All experiments were performed three or more times independently under similar conditions, except for experiments performed twice shown in Fig. 2i (the same observation was independently reproduced in Fig. 7d) and Fig. 5a,e, and Supplementary Figs 1I, 3B–D,G–I, 5F–I, 6E,G,H–J and 8D,H,I. Results are shown as mean and the error bars represent the standard error of the mean (s.e.m.), unless stated otherwise. Representative experiments are shown as the mean of technical triplicates. Prism 6 software was used to generate graphs and to perform statistical analysis. *P* values were calculated by chi-squared test or unpaired two-tailed Student's *t*-test as reported in the figure legends. *P* values of statistical significance are represented as $^{*}P < 0.05$, $^{**}P < 0.01$, $^{***}P < 0.001$, $^{****}P < 0.0001$.

Data availability. RNA-seq data are deposited in NCBI GEO (Gene Expression Omnibus) under accession number GSE75512. Statistical source data are shown in Supplementary Table 4. All other data supporting the findings of this study are available from the corresponding author on reasonable request.

51. Nojima, T., Gomes, T., Carmo-Fonseca, M. & Proudfoot, N. J. Mammalian NET-seq analysis defines nascent RNA profiles and associated RNA processing genome-wide. *Nat. Protoc.* **11,** 413–428 (2016).
52. Cawthon, R. M. Telomere measurement by quantitative PCR. *Nucleic Acids Res.* **30,** e47 (2002).
53. Berkovich, E., Monnat, R. J. Jr & Kastan, M. B. Roles of ATM and NBS1 in chromatin structure modulation and DNA double-strand break repair. *Nat. Cell Biol.* **9,** 683–690 (2007).
54. Dignam, J. D., Lebovitz, R. M. & Roeder, R. G. Accurate transcription initiation by RNA polymerase II in a soluble extract from isolated mammalian nuclei. *Nucleic Acids Res.* **11,** 1475–1489 (1983).
55. Langmead, B. & Salzberg, S. L. Fast gapped-read alignment with Bowtie 2. *Nat. Methods* **9,** 357–359 (2012).
56. Li, H. *et al.* The sequence alignment/map format and SAMtools. *Bioinformatics* **25,** 2078–2079 (2009).

© 2017 Macmillan Publishers Limited, part of Springer Nature. All rights reserved.

nature cell biology

DOI: 10.1038/ncb3643

In the format provided by the authors and unedited.

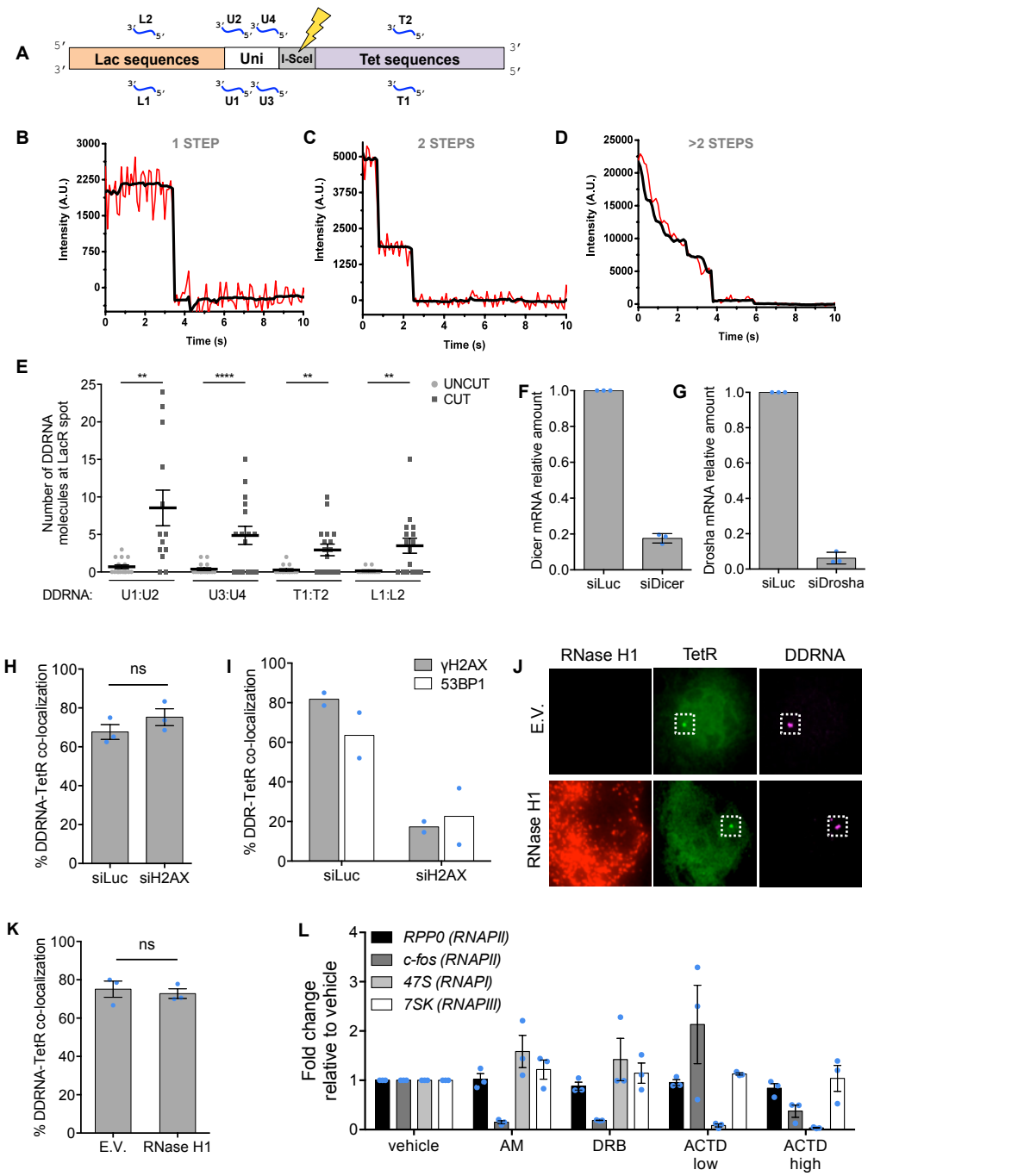

Supplementary Figure 1 Localization of DDRNAs at sites of DNA damage is not dependent on H2AX or DDRNA:DNA pairing. (**A**) Mapping of the synthetic DDRNA pairs (in blue) L1:L2, U1:U2, U3:U4, T1:T2 relative to the I-SceI cut site. (**B**-**D**) Examples of stepwise photobleaching traces of individual DDRNA particles co-localizing with GFP-LacR (relative to Fig. 1B). Raw intensity is depicted in red. Chung-Kennedy non-linear filter is represented in black. (**E**) Deconvolved DDRNAs display the same localization pattern of the DDRNA pool (relative to Fig. 1B). Plot represents the number of DDRNA molecules at the LacR spot as measured by single-molecule counting based on stepwise photobleaching of fluorescent probes. Dots represent individual cells. The black line represents the mean ± SEM (n=3 independent experiments). (**F, G**) Mean fold change of Dicer and Drosha mRNA in NIH2/4 cells by RT-qPCR. Error bars indicate SEM (relative to Fig. 1C, n=3 independent experiments). (**H**) DDRNA-Cy5 localization to the damaged site does not depend on H2AX in NIH2/4 cells. The bar plot shows the percentage of cells with DDRNA-TetR co-localization. Error bars indicate SEM (n=3 independent experiments, ≥80 cells analysed in total per condition). (**I**) Immunofluorescence analysis (relative to H) confirms reduced γH2AX and 53BP1 foci co-localization with YFP-TetR upon H2AX knockdown in cut NIH2/4 cells (mean of n=2 independent experiments, ≥40 cells analysed in total per condition). (**J**, **K**) DDRNA-Cy5 localization does not depend on DDRNA:DNA pairing. NIH2/4 cells were expressing YFP-TetR and I-SceI and RNase H1-expressing vector or an empty control vector (E.V.) were incubated with DDRNA-Cy5. Cells overexpressing RNase H1 were scored by staining with anti-RNase H1 antibody. In K, the bar plot shows the percentage of cells DDRNA-TetR co-localization. Error bars indicate SEM (n=3 independent experiments, ≥80 cells analysed in total per condition). (**L**) Mean fold change of the indicated RNAs in NIH2/4 cells by RT-qPCR. Error bars indicate SEM (relative to Fig. 1D, n=3 independent experiments). *P* values were calculated using chi-squared test. ns indicates not significant. Statistical source data are provided in Supplementary Table 4.

© 2017 Macmillan Publishers Limited, part of Springer Nature. All rights reserved.

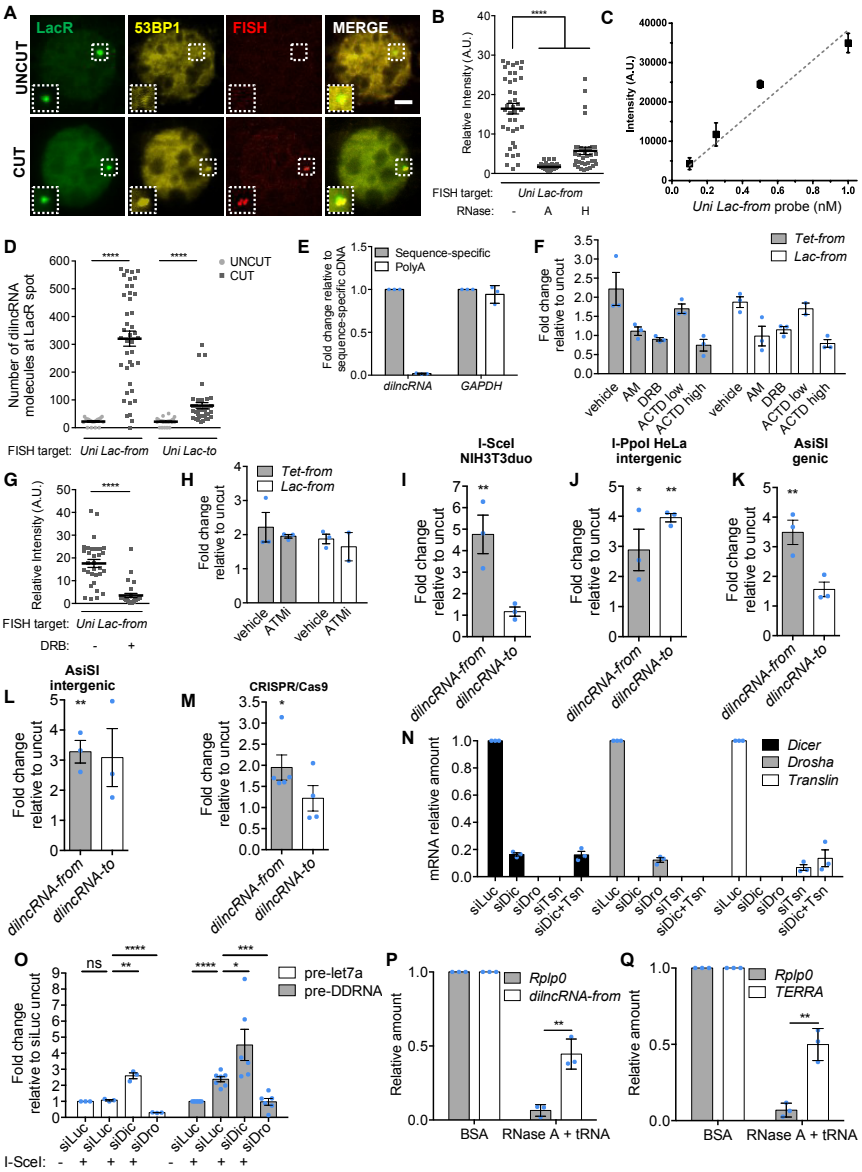

Supplementary Figure 2 Characterization of DSB-induced transcripts. (**A**) Representative images of FISH signal (red) on NIH2/4 cells transfected with GFP-LacR (green), 53BP1-mCherry (yellow) and pLacZ (uncut) or pI-SceI (cut). Scale bar 5μm. Inset is a magnified view (relative to Fig. 2B, representative of 3 independent experiments). (**B**) Plot shows the relative intensity of Uni Lac-from FISH probe. When indicated, RNase A or RNase H treatment was performed prior or after DNA probe hybridization, respectively. Dots represent individual cells. Black bar represents mean ± SEM (n=3 independent experiments). (**C**) Uni Lac-from probe at various concentrations (0.1-1 nM) was used with the same acquisition parameters as FISH samples. Linear fit is depicted as a grey dotted line (R2 = 0.92). Error bars show SD (n=5 regions/slide, 2 slides). (**D**) Plot represents the number of transcripts at locus, based on the FISH signal intensity of Uni Lac-from and Uni Lac-to probes. Dots represent individual cells. Black bar represents mean ± SEM (n=3 independent experiments). (**E**) DilncRNAs are non-polyadenylated RNAs. Total RNA extracted from NIH2/4 cells was reverse-transcribed with oligo-dT or sequence-specific primers and dilncRNA and GAPDH mRNA were detected by RT-qPCR. RT with sequence-specific primer was used as reference. Error bars indicate SEM (n=3 independent experiments). (**F**) Strand-specific RT-qPCR shows that DSB-dependent transcription is sensitive to RNAPII inhibition. Bar plot shows the fold change relative to vehicle-treated samples of the indicated RNAs in cells treated AM, DRB, ACTD at low or high doses for 2 h before I-SceI induction. Error bars indicate SEM (n=3 independent experiments). (**G**) FISH signal relative intensity of Uni Lac-from probe upon DRB treatment. Dots represent individual cells. Black bar represents the mean ± SEM (n=3 independent experiments). (**H**) DSB-induced transcription is not dependent on ATM kinase activity. Bar plot shows the mean fold change respect to uncut of the indicated dilncRNAs in NIH2/4 cells treated with ATM inhibitor (KU60019 10μM) or DMSO for 16h before cut. Error bars indicate SEM (n=3 independent experiments). (**I-M**) Strand-specific-RT-qPCR showing dilncRNA-from and dilncRNA-to in different cell lines upon DSB induction. Bar plots show the mean fold change respect to uncut. Error bars indicate SEM. (I) NIH3T3duo cells cut by I-SceI (n=3 independent experiments); (J) HeLa cells cut by I-PpoI in an intergenic site (n=3 independent experiments); (K) U2OS cells cut by AsiSI in a genic site (n=3 independent experiments); (L) BJ cells cut by AsiSI in an intergenic site (n=3 independent experiments); (M) NIH2/4 cells cut by CRISPR/Cas9 at the *c-Myc* locus (n=4 independent experiments). (**N**) Mean fold change of Drosha, Dicer and Translin mRNA by RT-qPCR in NIH2/4 cells. Error bars indicate SEM (n=3 independent experiments). (**O**) Pre-DDRNA and pre-miRNA have a similar biogenesis. NIH2/4 cells knocked-down for Drosha (siDro), Dicer (siDic) or Luciferase (siLuc) were transfected with a vector expressing I-SceI (+) or an empty vector (-). RNA fractions of 40-200 nt in length were recovered by gel-extraction. Bar plots show the relative enrichment of let7a pre-miRNA and Lac pre-DDRNA. Error bars indicate SEM (n=3 independent experiments). (**P, Q**) DilncRNAs and the chromatin-bound ncRNA-*TERRA* are resistant to RNase A. Bar plots show the mean fold change of the indicated RNAs upon RNase A treatment relative to BSA-treated sample. Error bars indicate SEM (n=3 independent experiments). *P* value was calculated using two-tailed t-test. **P*<0.05, ***P*<0.01, ****P*<0.001, **** *P*<0.0001. Statistical source data are provided in Supplementary Table 4.

© 2017 Macmillan Publishers Limited, part of Springer Nature. All rights reserved.

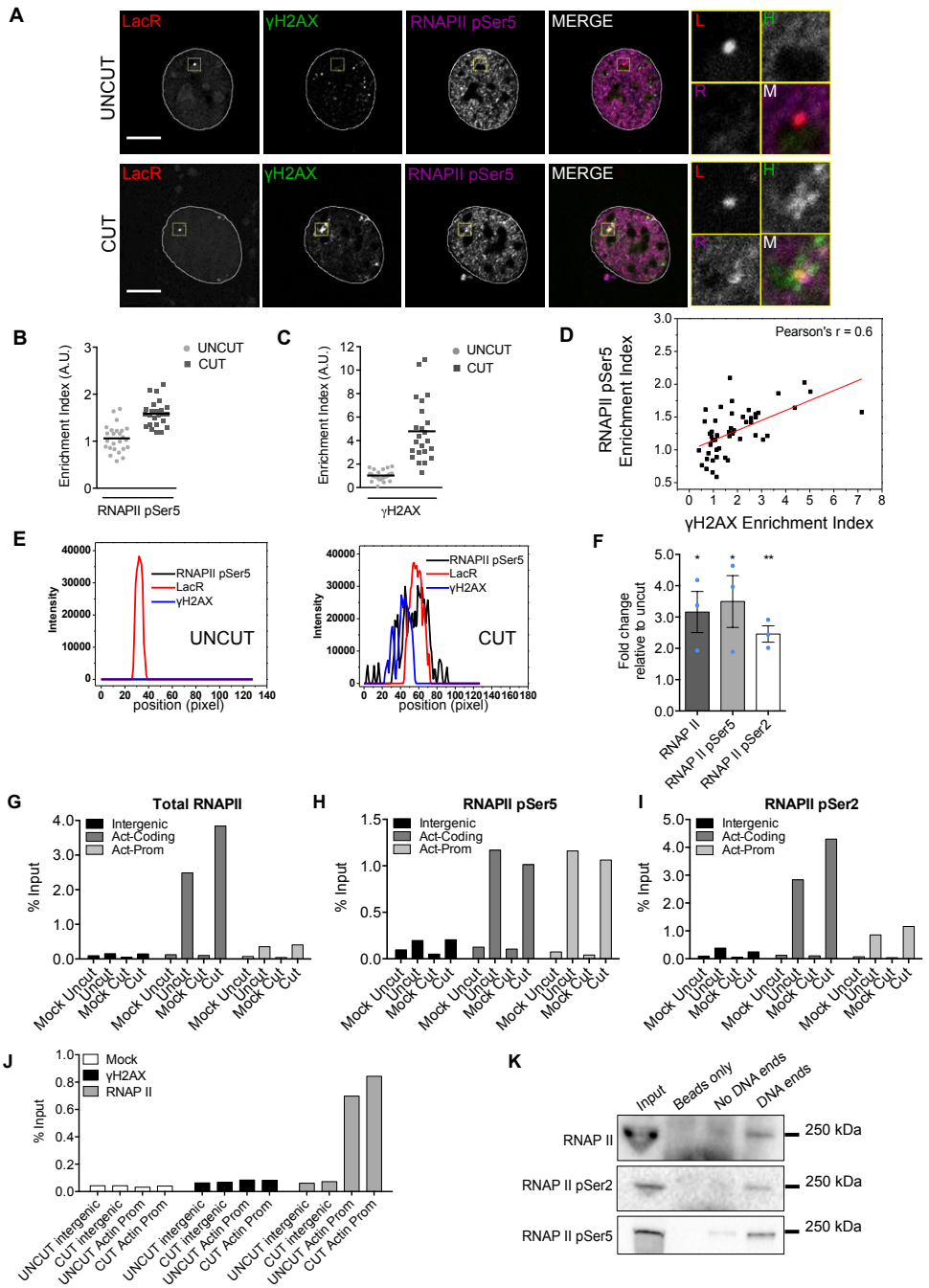

Supplementary Figure 3 RNAPII localizes to DSBs in mammalian cells. (**A**) Confocal microscopy reveals the enrichment of γH2AX and active RNAPII at the damaged locus. The panel shows representative confocal images of LacR loci (red, inset L), γH2AX (green, inset H), RNAPII pSer5 (purple, inset R) and merge (inset M) in uncut and cut NIH2/4 cells. The yellow-boxed inset images correspond to the yellow-boxed regions. White outline defines nuclear contour. Scale bar 10 μm. (**B**, **C**) Quantification of (A). Plots show the enrichment of RNAPII pSer5 and γH2AX in uncut and cut cells, calculated on confocal image stacks. Dots represent individual cells. Black bar represents mean (data are shown as pool of 2 independent experiments, ≥25 cells per sample). (**D**) RNAPII pSer5 enrichment index was plotted as a function of γH2AX enrichment index at the Cherry-LacR signal. Linear fit is depicted as a red line (Pearson's r = 0.6). Individual data points correspond to individual nuclei (data are shown as pool of 2 independent experiments, ≥50 nuclei). (**E**) Intensity profiles along the chromatin fibers in the yellow-boxed images in Fig. 3A. (**F**) Bar plot shows the mean fold change relative to uncut cells of RNAPII pSer5 and pSer2 and total RNAPII enrichment at the Lac sequences in NIH2/4. Error bars indicate SEM (n=3 independent experiments). (**G-I**) ChIP controls in NIH2/4 cells. RNAPII pSer5 and pSer2 and total RNAPII are enriched in the coding and promoter regions of the beta-actin (Act) gene, but not in an intergenic region. Data are shown as percentage of input. Data are shown as one representative of 2 independent experiments. (**J**) ChIP controls in HeLa cells. Total RNAPII is enriched in the coding and promoter regions of the beta-actin (Act) gene, but not in an intergenic region. Data are shown as percentage of input. Data are shown as one representative of 3 independent experiments. (**K**) Biotinylated DNA on streptavidin beads was cut or not by recombinant I-SceI and incubated with nuclear cell extract. Input and pull-down samples were probed for total RNAPII pSer5 and pSer2 and total RNAPII. *P* value was calculated using two-tailed t-test. **P*<0.05, ***P*<0.01, *****P*<0.0001. Statistical source data are provided in Supplementary Table 4. Unprocessed original blots are shown in Supplementary Figure 9.

© 2017 Macmillan Publishers Limited, part of Springer Nature. All rights reserved.

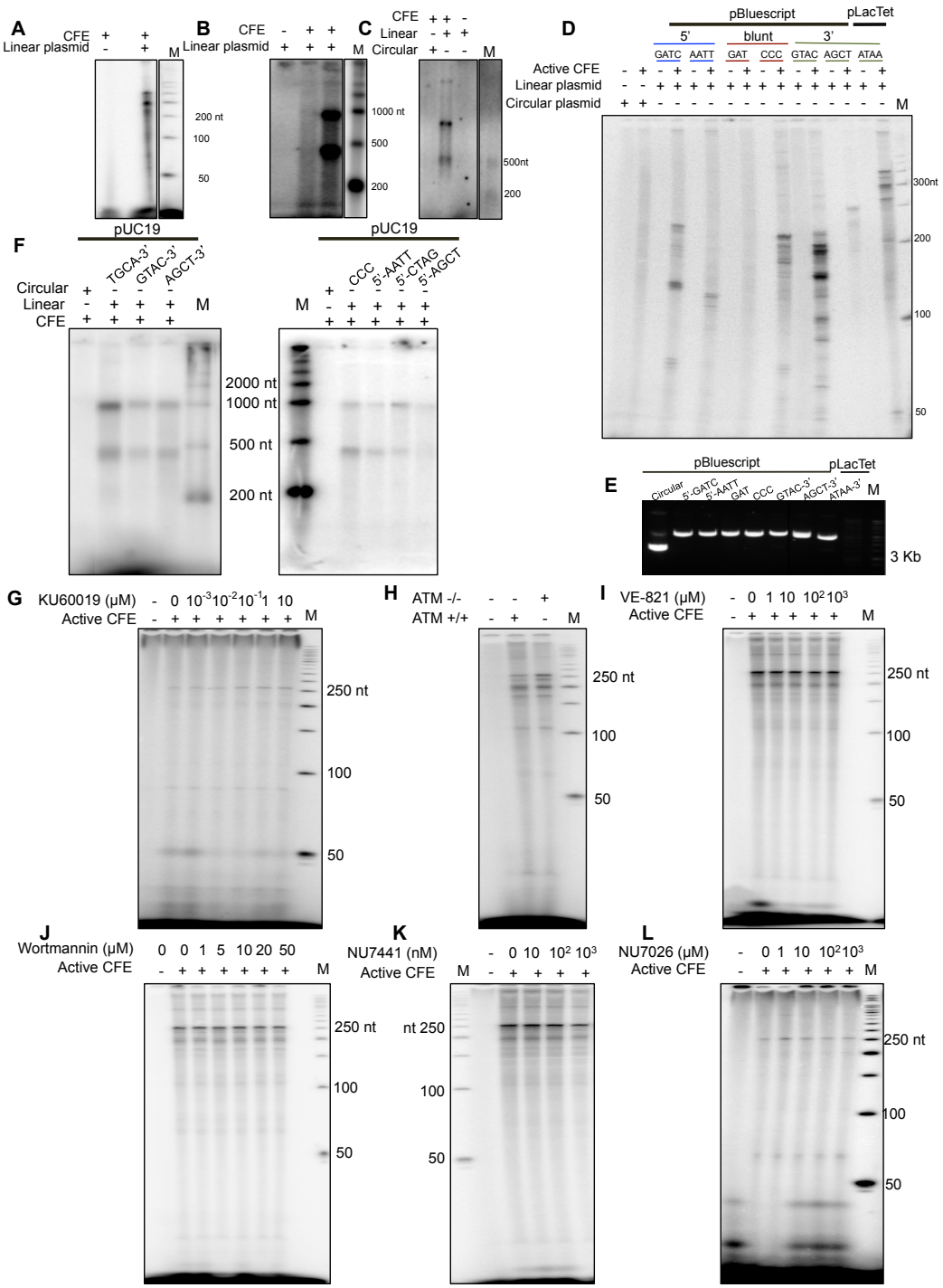

Supplementary Figure 4 *In vitro* DSB-induced transcription is not dependent on DDR kinases. (**A**-**C**) Denaturing PAGE showing the products of *in vitro* transcription reactions in the presence of [α^{32}P]UTP with pLacTet plasmid (A) or pUC19 plasmid (B,C) and appropriate controls. CFE indicates cell free extract. M indicates radiolabeled DNA ladder, nt indicates nucleotides. (**D**) Denaturing PAGE showing the products of in vitro transcription reactions in the presence of [α^{32}P]UTP with pBluescript plasmid in its circular form or digested with different restriction enzymes generating one DSB with 5'-protruding, blunt or 3'-protruding DNA ends. pLacTet plasmid is used as control. CFE indicates cell free extract. M indicates radiolabeled DNA ladder, nt indicates nucleotides. (**E**) Agarose gel shows equal amounts of DNA used in (D). (**F**) Denaturing PAGE showing the products of in vitro transcription reactions in the presence of [α^{32}P]UTP with pUC19 plasmid in its circular form or digested with different restriction enzymes, as in (D). (**G**-**L**) Analysis of the role of DDR upstream kinases in the control of transcription from DSBs. Denaturing PAGE showing in vitro transcription assays performed by incubating cell-free extract (CFE) with linear pLacTet plasmid and increasing concentrations (0, 1, 10, 100 nM, 1, 10 μM) of the ATM inhibitor KU60019 (G); with cell-free extract (CFE) prepared from ATM wild-type or knockout embryonic stem (ES) cells (H); with increasing concentrations (0, 1, 10, 100, 1000 μM) of the ATR inhibitor VE-821 (I); with increasing concentrations (0,1, 5, 10, 20, 50 μM) of the PI3K-like kinases inhibitor Wortmannin (J); with increasing concentrations of the following DNA-PKcs inhibitors: (K) NU7441 (0, 10, 100, 1000 nM) and (L) NU7026 (0, 1, 10, 100, 1000 μM). M indicates radiolabeled DNA ladder, nt indicates nucleotides.

© 2017 Macmillan Publishers Limited, part of Springer Nature. All rights reserved.

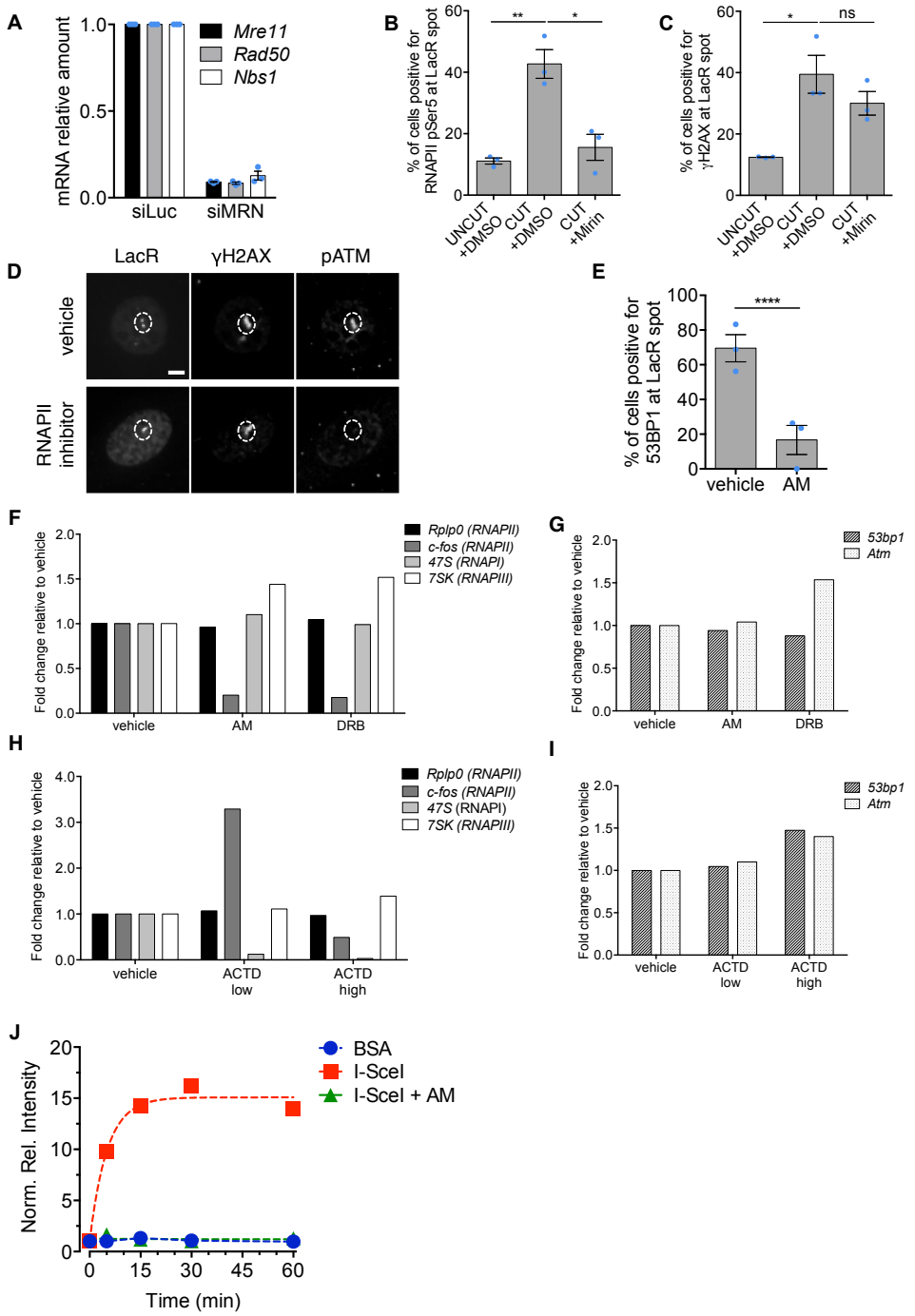

Supplementary Figure 5 The MRN complex is necessary for RNAPII recruitment to DSBs and DDR foci are sensitive to RNAPII inhibition. (**A**) Analysis by RT-qPCR shows a significant reduction in *Mre11*, *Rad50* and *Nbs1* mRNA relative levels upon knockdown by siRNA (siMRN) in NIH2/4 cells. Error bars represent SEM (n=3 independent experiments). (**B**, **C**) The bar plots show the enrichment of RNAPII pSer5 and γH2AX in uncut and cut cells treated with DMSO or Mirin, calculated on confocal image stacks. Data is shown as mean. Error bars represent SEM (n=3 independent experiments). (**D**) Focal accumulation of pATM, but not γH2AX, at the damage site is reduced in cut NIH2/4 cells treated with RNAPII inhibitor. The panel shows representative images of NIH2/4 cells treated with vehicle or RNAPII inhibitor before induction of I-SceI. Scale bar 5 μm. (**E**) Specific inhibition of RNAPII by a 6 h treatment with AM before cut induction strongly inhibits 53BP1 focus formation at the locus in NIH2/4 cells. The bar plot shows the percentage of cells positive for 53BP1-LacR co-localization. Error bars indicate SEM (n=3 independent experiments, ≥60 cells per sample). (**F**-**I**) Efficacy as well as specificity of AM, DRB, ACTD treatments in NIH2/4 cells were evaluated by RT-qPCR by quantifying short-lived RNAs specifically transcribed by individual RNA polymerases, as indicated, as well as *53bp1* and *Atm* mRNA levels. The bar plots show the levels of the indicated RNA. Data are shown as one representative of 2 independent experiments. (**J**) NIH2/4 cells transfected with GFP-LacR and Cherry-53BP1 were microinjected either with BSA, I-SceI or I- SceI together with AM. The plot shows the relative intensity of 53BP1 focus over time (min) in the different conditions. Data are normalized to the 0 min time point for each sample (≥10 cells per time point, per sample). (B, C) *P* value was calculated using two-tailed t-test. (E) *P* value was calculated using chi-squared test. **P*<0.05, ***P*<0.01, *****P*<0.0001. ns indicates not significant. Statistical source data are provided in Supplementary Table 4.

© 2017 Macmillan Publishers Limited, part of Springer Nature. All rights reserved.

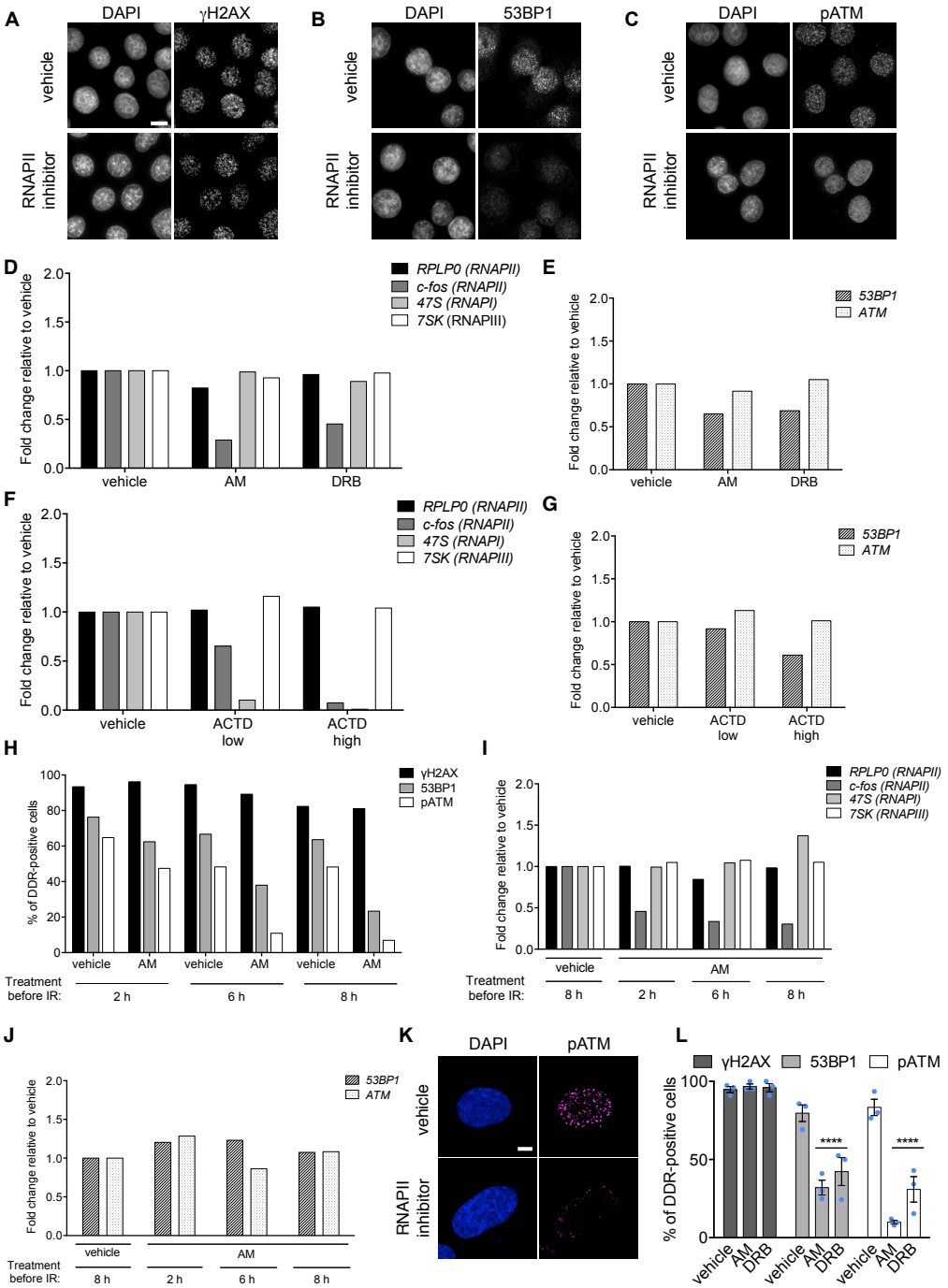

Supplementary Figure 6 IR-induced DDR foci are sensitive to RNAPII inhibition. (**A**-**C**) Focal accumulation of 53BP1 and pATM, but not γH2AX, upon IR is reduced in HeLa cells treated with RNAPII inhibitors (relative to Fig. 6E, F). Representative images of HeLa treated with vehicle or RNAPII inhibitors (AM in these images) before IR and probed for γH2AX, 53BP1 and pATM. Scale bar 10μm. (**D**-**G**) HeLa cells were treated with AM for 6h, DRB, ACTD at low or high doses for 2 h before IR and RNA was extracted 1h post IR. Efficacy of the treatments were evaluated by RT-qPCR by quantifying short-lived RNAs specifically transcribed by individual RNA polymerases, as indicated, as well as *53BP1* and *ATM* mRNA levels. The bar plots show the levels of the indicated RNA. Data are shown as one representative of 4 (D, F) or 2 (E, G) independent experiments. (**H**) Bar plot shows the percentage of irradiated HeLa cells positive for γH2AX, 53BP1 and pATM upon different treatments with AM (cells with >10 foci were scored positive, >100 cells per sample). (**I**, **J**) Efficacy as well as specificity of the treatments with AM for 2, 6 and 8h were evaluated by RT-qPCR by quantifying short-lived RNAs specifically transcribed by individual RNA polymerases, as indicated, as well as *53BP1* and *ATM* mRNA levels. The bar plots show the levels of the indicated RNA. Data are shown as one representative of 2 independent experiments. (**K**) pATM foci are reduced in irradiated normal human fibroblasts (BJ) treated with RNAPII inhibitors. The panel shows representative images of cells treated with vehicle or RNAPII inhibitor (DRB in these images) 2h before IR. Scale bar 5μm. (**L**) BJ cells were treated with AM, DRB or vehicle 2h before IR. Bar plot (quantification of Fig. 6D and Supplementary Fig. 6K) shows the percentage of cells positive for γH2AX, 53BP1 and pATM (cells with >10 foci were scored positive). Error bars indicate SEM (n=3, n>100 cells per sample). *P* value was calculated using two-tailed t-test. ***P*<0.01, ****P*<0.001, *****P*<0.0001. Statistical source data are provided in Supplementary Table 4.

© 2017 Macmillan Publishers Limited, part of Springer Nature. All rights reserved.

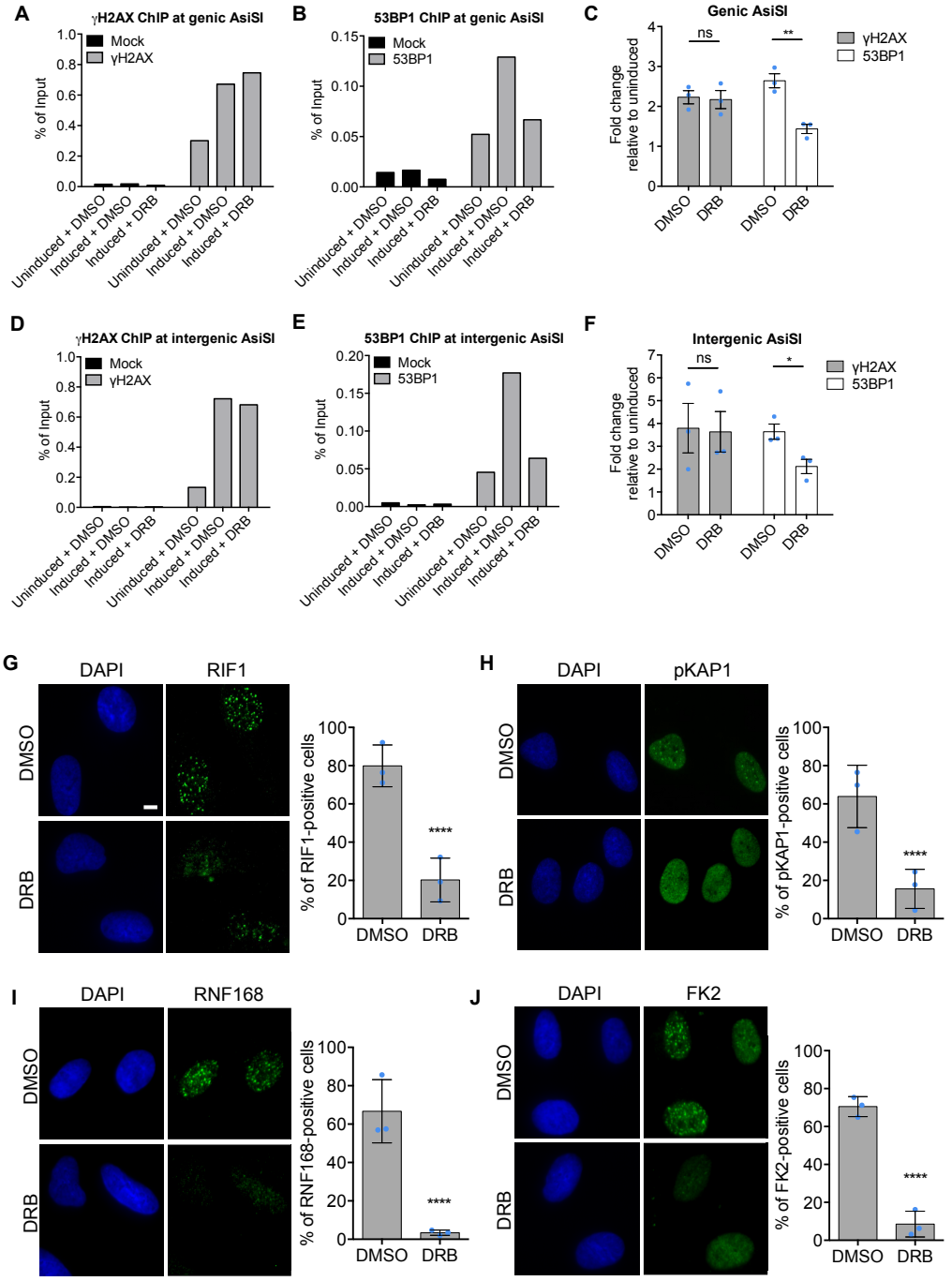

Supplementary Figure 7 IR-induced DDR foci are sensitive to RNAPII inhibition in normal human fibroblasts. (**A, B**) Accumulation of 53BP1, but not γH2AX, to an AsiSI-induced DSB is impaired in AsiSI-ER BJ-5Ta cells treated with DRB at a genic site. The bar plots show the percentage of ChIP enrichment relative to the input of γH2AX (A) and 53BP1 (B) associated with genomic DNA. Data are shown as one representative of 3 independent experiments. (**C**) Fold change relative to uninduced cells of γH2AX and 53BP1 enrichment at a genic site (relative to A, B). Values are shown as mean. Error bars indicate SEM (n=3 independent experiments). (**D, E**) Same analyses as in (A, B) at an AsiSI-ER intergenic site. Data are shown as one representative of 3 independent experiments. (**F**) Fold change relative to uninduced cells of γH2AX and 53BP1 enrichment at an intergenic site (relative to D, E). Values are shown as mean. Error bars indicate SEM (n=3 independent experiments). (**G-J**) Foci of RIF1 (G), pKAP1 (H), RNF168 (I) and ubiquitinylated proteins detected by FK2 antibody (J) are reduced in irradiated normal human fibroblasts (BJ) treated with DRB for 2h at RT before IR. The panel shows representative images. Scale bar 5μm. The bar plot shows the percentage of positive cells (cells with >10 foci for RIF1, RNF168 and FK2 and >3 foci for pKAP1 were considered positive). Error bars indicate SEM (n=3 independent experiments, >150 cells per sample). *P* value was calculated using two-tailed t-test. **P*<0.05, ***P*<0.01, *****P*<0.0001. ns indicates not significant. Statistical source data are provided in Supplementary Table 4.

© 2017 Macmillan Publishers Limited, part of Springer Nature. All rights reserved.

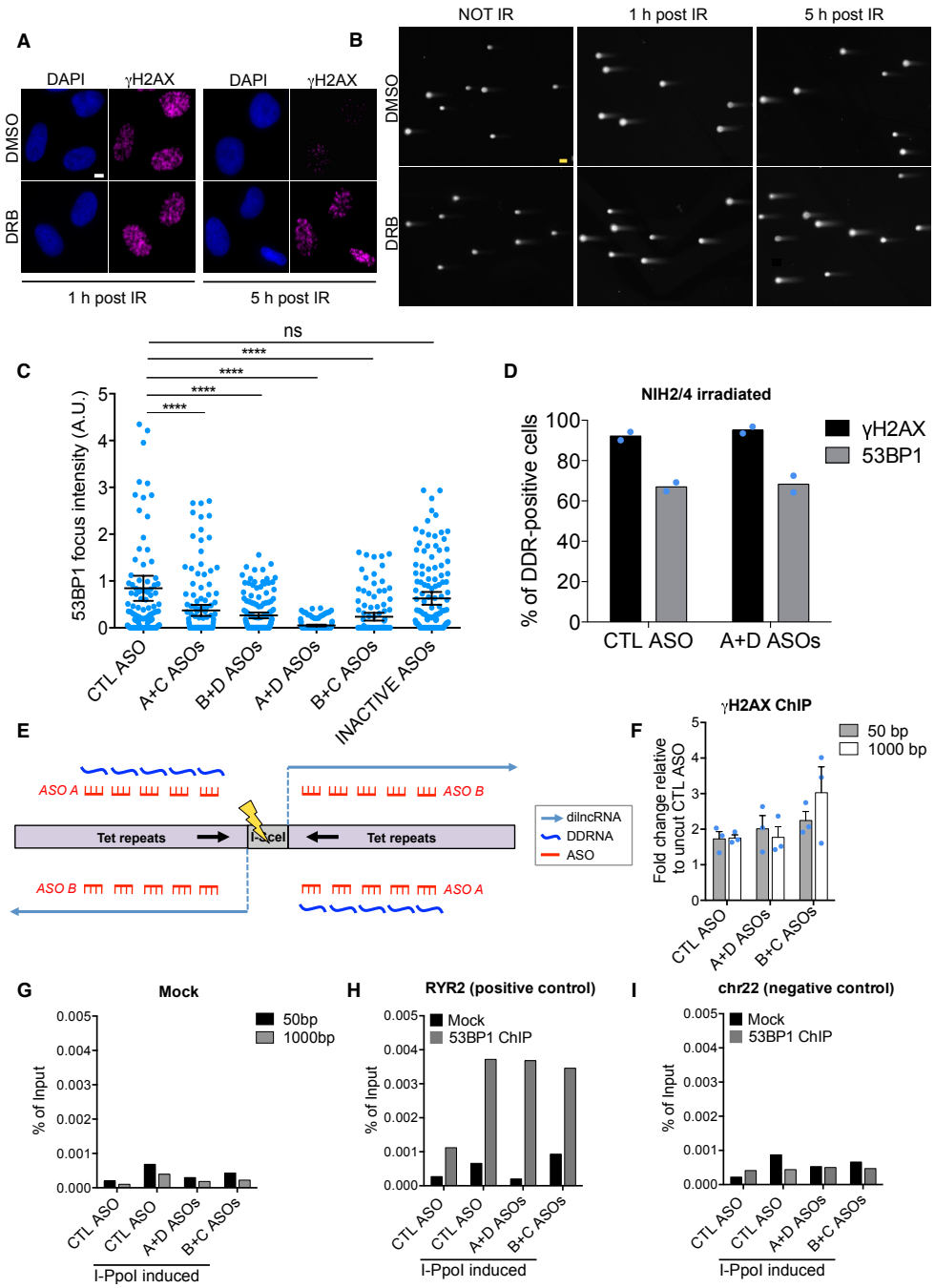

Supplementary Figure 8 RNAPII inhibition impairs DNA repair and sequence-specific ASOs reduce DDR foci formation at individual DSBs. (**A**) Representative images of BJ cells pre-treated with DMSO or DRB for 2 h, irradiated (2Gy) and fixed at the indicated time points (relative to Fig. 6G). Scale bar 5μm (**B**) Representative images of neutral comet assay. HeLa cells were pre-treated with DMSO or DRB for 2 h, irradiated (5Gy) and collected at the indicated time points (relative to Fig. 7H, I). Scale bar 20μm (**C**) Quantitative analysis of 53BP1 focus intensity, normalized on Mock sample, of the experiments shown in Fig. 7D. Dots represent individual cells. Black bar represents mean. Error bars indicate SEM (data are shown as pool of n=3 independent experiments, ≥100 cells analysed for each sample). (**D**) NIH2/4 cells were transfected with the indicated ASOs, irradiated (2Gy) and fixed 1 h post IR. Bar plot shows the percentage of DDR-positive cells (mean of n=2 independent experiments, >50 cells per sample). (**E**) Schematic representation of ASOs (A and B in red) preventing the interaction between dilncRNAs (light blue) and DDRNAs (dark blue) originating from Tet sequences in NIH3T3duo cell line. The black arrows indicate the head-to-head configuration of Tet sequences flanking the I-SceI site. (**F**) Bar plot shows mean fold change normalized to uncut CTL ASO of enrichment relative to input of γH2AX at *DAB1* locus at 50, 1000 bp from DSB. Error bars indicate SEM (n=3 independent experiments). (**G**) Bar plot shows the percentage of enrichment relative to the input of Mock sample at *DAB1* locus at 50, 1000 bp from DSB. Data are shown as one representative of 3 independent experiments. (**H**) Bar plot shows the percentage of enrichment relative to the input of 53BP1 or Mock at *RYR2* locus cut by I-PpoI in HeLa cells. Data are shown as one representative of 2 independent experiments. (**I**) Bar plot shows the percentage of enrichment relative to the input of 53BP1 or Mock at an unrelated region on chromosome 22 not cut by I-PpoI in HeLa cells. Data are shown as one representative of 2 independent experiments. *P* value was calculated using two-tailed t-test. ****$P<0.0001$. ns indicates not significant. Statistical source data are provided in Supplementary Table 4.

© 2017 Macmillan Publishers Limited, part of Springer Nature. All rights reserved.

Unprocessed blots relative to Figure 5A

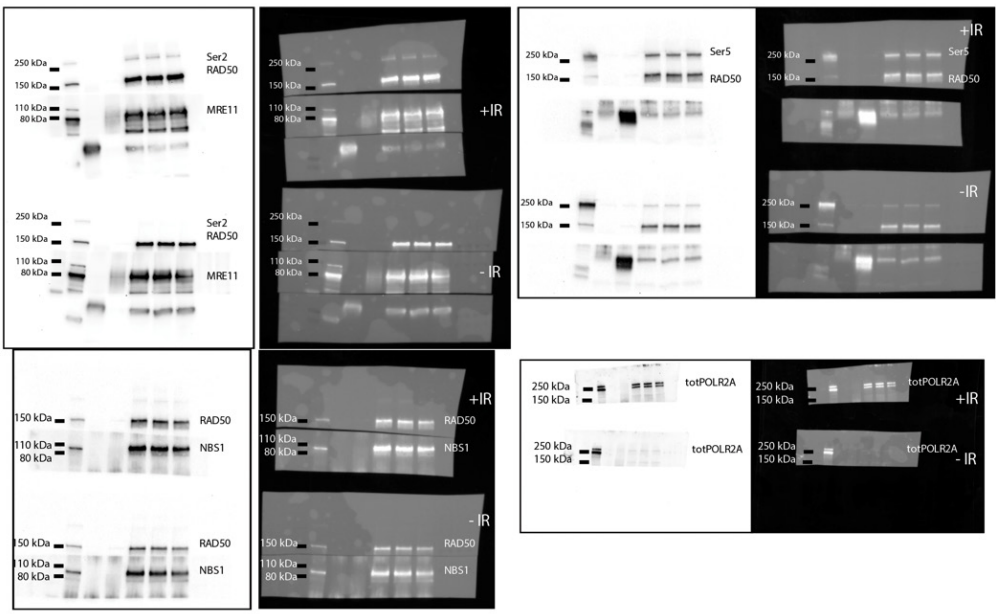

Unprocessed blot relative to Figure 3E

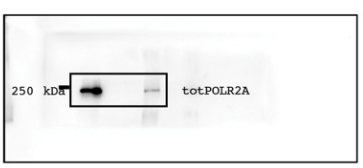

Unprocessed blots relative to Supplementary Figure 3K

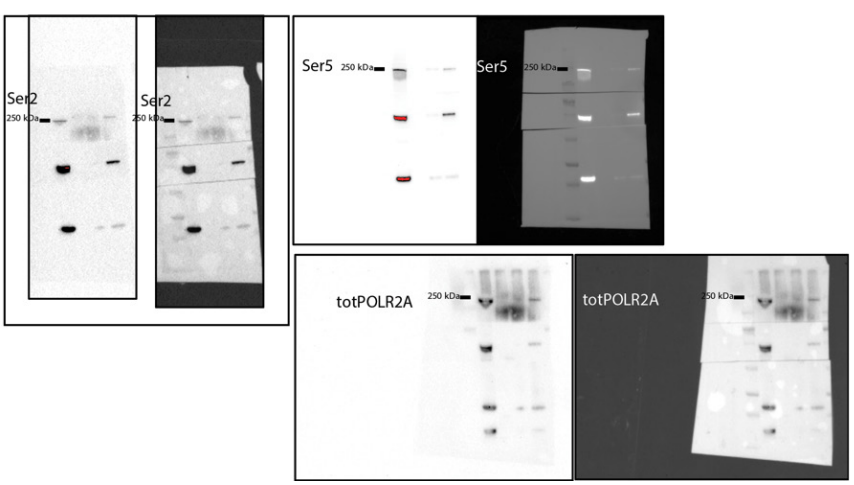

Supplementary Figure 9 Unprocessed blots. Unprocessed blots relative to Figures 3E, 5A and Supplementary Figure 3K.

© 2017 Macmillan Publishers Limited, part of Springer Nature. All rights reserved.

Supplementary Table Legends

Supplementary Table 1 Sequences of primers and probes.

Supplementary Table 2 Sequences of RNA oligonucleotides and siRNA.

Supplementary Table 3 Sequences of antisense oligonucleotides.

Supplementary Table 4 Statistical source data.

© 2017 Macmillan Publishers Limited, part of Springer Nature. All rights reserved.

nature research

Corresponding author(s): Fabrizio d'Adda di Fagagna

☐ Initial submission ☐ Revised version ☒ Final submission

Life Sciences Reporting Summary

Nature Research wishes to improve the reproducibility of the work that we publish. This form is intended for publication with all accepted life science papers and provides structure for consistency and transparency in reporting. Every life science submission will use this form; some list items might not apply to an individual manuscript, but all fields must be completed for clarity.

For further information on the points included in this form, see Reporting Life Sciences Research. For further information on Nature Research policies, including our data availability policy, see Authors & Referees and the Editorial Policy Checklist.

Experimental design

1. Sample size

Describe how sample size was determined.

Sample size was not pre-determined.
For imaging analyses of irradiation-induced DDR foci, on average 100 cells per sample were analyzed in each experiment unless stated differently in figure legends. For single-cell high-resolution or confocal imaging analyses, on average 30 cells per sample were analyzed in each experiment unless stated differently in figure legends.
Sample size and number of independent experiments are always clearly stated in the figure legend or in the Methods section.

2. Data exclusions

Describe any data exclusions.

Throughout the manuscript no data was excluded, only in the case of high resolution DDRNA-Cy5 and smFISH analyses, cells with more than one Lac-GFP spot were excluded because indicative of spurious recombination events.

3. Replication

Describe whether the experimental findings were reliably reproduced.

All experiments were repeated at least 3 times, unless stated differently in figure legends. The main observations of the work were reproduced in different cell lines (human and mouse), in different experimental settings (in cells or cell extracts) and by different technologies (IF, smFISH, ChIP, qRT-PCR).
Sample size and number of independent experiments are clearly stated in the figure legend or in the Methods section.

4. Randomization

Describe how samples/organisms/participants were allocated into experimental groups.

No randomization method was used.

5. Blinding

Describe whether the investigators were blinded to group allocation during data collection and/or analysis.

Investigators were not blinded to group allocation during data collection and analysis. However, whenever applicable, quantification of the intensity or the number of foci per nucleus was performed in an unbiased way with the automated image-analysis software CellProfiler 2.1.1 or ImageJ as stated in the Methods section.

Note: all studies involving animals and/or human research participants must disclose whether blinding and randomization were used.

6. Statistical parameters

For all figures and tables that use statistical methods, confirm that the following items are present in relevant figure legends (or in the Methods section if additional space is needed).

n/a	Confirmed
☐	☒ The exact sample size (*n*) for each experimental group/condition, given as a discrete number and unit of measurement (animals, litters, cultures, etc.)
☐	☒ A description of how samples were collected, noting whether measurements were taken from distinct samples or whether the same sample was measured repeatedly
☐	☒ A statement indicating how many times each experiment was replicated
☐	☒ The statistical test(s) used and whether they are one- or two-sided (note: only common tests should be described solely by name; more complex techniques should be described in the Methods section)
☐	☒ A description of any assumptions or corrections, such as an adjustment for multiple comparisons
☒	☐ The test results (e.g. *P* values) given as exact values whenever possible and with confidence intervals noted
☐	☒ A clear description of statistics including central tendency (e.g. median, mean) and variation (e.g. standard deviation, interquartile range)
☐	☒ Clearly defined error bars

See the web collection on statistics for biologists for further resources and guidance.

Software

Policy information about availability of computer code

7. Software

Describe the software used to analyze the data in this study.

MetaMorph software was used to acquire widefield images. Quantification of the number of nuclear foci per nucleus was performed with the automated image analysis software CellProfiler 2.1.1.
DeltaVision images were automatically subjected to deconvolution by softWoRx software.
For super-resolution data analysis, raw data were processed using Zeiss Zen software to detect single-molecule events above background noise.
ImageJ and Fiji softwares were used to analyze and pseudocolor images.
Comet tail moment was calculated using OpenComet software.
Deep sequencing reads were mapped using Bowtie2 software.

For manuscripts utilizing custom algorithms or software that are central to the paper but not yet described in the published literature, software must be made available to editors and reviewers upon request. We strongly encourage code deposition in a community repository (e.g. GitHub). *Nature Methods* guidance for providing algorithms and software for publication provides further information on this topic.

Materials and reagents

Policy information about availability of materials

8. Materials availability

Indicate whether there are restrictions on availability of unique materials or if these materials are only available for distribution by a for-profit company.

Unique materials are available upon request.

9. Antibodies

Describe the antibodies used and how they were validated for use in the system under study (i.e. assay and species).

Primary antibodies for immunofluorescence: γH2AX pS139 (mouse, Millipore 05-636, 1:1000); ATM pS1981 (mouse, Rockland 200-301-400, 1:400); 53BP1 (rabbit, Novus Biologicals NB100-304, 1:1000); RNAPII pSer5 (rabbit, Abcam ab5131, 1:500); RNaseH1 (rabbit, Proteintech 15606-1-AP, 1:200); RIF1 (rabbit, Bethyl A300-569A, 1:1000), pKAP1 (rabbit, Bethyl A300-767A, 1:1000), RNF168 (rabbit, Millipore Abe367, 1:500), mono- and polyubiquitinylated conjugates monoclonal antibody (FK2, Enzo life sciences BML-PW8810-0100, 1:1000). Secondary antibodies for immunofluorescence: donkey anti-mouse or anti-rabbit Alexa 405 (1:200), Alexa 488 (1:500) or Alexa 647 (1:500) IgG (Life Technologies) or goat anti-mouse or anti-rabbit Cy5 (Jackson Immunoresearch). The following antibodies were used for ChIP: RNAPII N-20 (rabbit, SantaCruz, sc899x, 2µg) four mouse cells; total RNAPII (mouse, Abcam, ab817, 5µg); RNAPII pSer2 (rabbit, Abcam ab5095, 2µg) for human cells; RNAPII pSer5 (rabbit, Abcam ab5131, 2µg); γH2AX pS139 (rabbit, Abcam ab2893, 2µg); 53BP1 (rabbit, Novus Biologicals NB100-305, 3µg). Primary antibodies for immunoprecipitation and western blot: RNAPII (POLR2A) (mouse, Santa Cruz 8WG16, IP: 5 µg/1mg of total proteins, WB: 1:50); MRE11 (rabbit polyclonal raised against recombinant human MRE11, gift from S. P. Jackson. Validation data using MRE11-deficient cells or purified recombinant MRN are available upon request. IP: 1 µg/1mg of total proteins, WB: 1:000); NBS1 (rabbit, Novus Biologicals NB100-143 IP: 1 µg/1mg of total proteins, WB: 1:000); RAD50 (Millipore (13B3/2C6) 05-525 IP: 1 µg/1mg of total proteins, WB: 1:000); RNAPII pSer2 (rabbit, Abcam ab5095 WB: 1:1000); RNAPII pSer5 (rabbit, Abcam ab5131 WB: 1:1000).

10. Eukaryotic cell lines

a. State the source of each eukaryotic cell line used.

NIH2/4 cells (Soutoglou et al., 2007)
NIH3T3duo cells (Roukos et al., 2013)
U2OS19ptight (Lemaitre et al., 2012)
AsiSI-ER-U20S cells (Iacovoni et al. 2010)
To generate AsiSI-ER BJ-5Ta cell line, BJ hTERT Hygro (ATCC, BJ-5Ta) were infected with pBABE HA–AsiSI–ER plasmid (from G. Legube)
HeLa cells (ATCC)
HeLa111 cells (Lemaitre et al., 2014)
Human normal foreskin fibroblast (BJ, ATCC)

b. Describe the method of cell line authentication used.

Cell lines are authenticated at each batch freezing by STR profiling (StemElite ID System, Promega).

c. Report whether the cell lines were tested for mycoplasma contamination.

All cell lines are are tested for mycoplasma at each batch freezing with both PCR (C C Uphoff, H G Drexler "Detecting mycoplasma contamination in cell cultures by polymerase chain reaction" , Methods in Molecular medicine 88: Cancer cell culture: methods and protocols, 319-326.) and a biochemical test (MycoAlert, Lonza)

d. If any of the cell lines used are listed in the database of commonly misidentified cell lines maintained by ICLAC, provide a scientific rationale for their use.

No commonly misidentified cell lines were used.

Animals and human research participants

Policy information about studies involving animals; when reporting animal research, follow the ARRIVE guidelines

11. Description of research animals

Provide details on animals and/or animal-derived materials used in the study.

No animals were used.

Policy information about studies involving human research participants

12. Description of human research participants

Describe the covariate-relevant population characteristics of the human research participants.

The study did not involve human research participants.